

A New Operational Mediterranean Diurnal Optimally Interpolated SST Product within the Copernicus Marine Environment Monitoring Service

Andrea Pisano¹, Daniele Ciani¹, Salvatore Marullo^{1,2} Rosalia Santoleri¹, Bruno Buongiorno Nardelli³

¹CNR-ISMAR, Via del Fosso del Cavaliere 100, Rome, 00133, Rome, Italy

²ENEA, Via Enrico Fermi, 45, 00044 Frascati, Italy

³CNR-ISMAR, Calata Porta di Massa, Napoli, 80133, Italy

Correspondence to: Andrea Pisano (andrea.pisano@cnr.it)

Abstract. Within the Copernicus Marine Environment Monitoring Service (CMEMS), a new operational MEDiterranean Diurnal Optimally Interpolated Sea Surface Temperature (MED DOISST) product has been developed. This product provides hourly mean maps (Level-4) of sub-skin SST at 1/16° horizontal resolution over the Mediterranean Sea from January 2019 to present. Sub-skin is the temperature at ~1 mm depth of the ocean surface, and then potentially subject to a large diurnal cycle. The product is built by combining hourly SST data from the Spinning Enhanced Visible and InfraRed Imager (SEVIRI) on board Meteosat Second Generation and model analyses through optimal interpolation. SEVIRI and model data are respectively used as the observation source and first-guess. The choice of using a model output as first-guess represents an innovative alternative to the commonly adopted climatologies or previous analyses, providing physically consistent estimates of hourly SSTs in the absence of any observation or in situ measurement. The accuracy of the MED DOISST product is assessed here by comparison against surface drifting buoy measurements, covering the years 2019 and 2020. The diurnal cycle reconstructed from DOISST is in good agreement with the one observed by independent drifter data, with a mean bias of 0.041 ± 0.001 K and root-mean-square difference (RMSD) of 0.412 ± 0.001 K. The new SST product is more accurate than the input model during the central warming hours, when the model, on average, underestimates drifter SST by one tenth of degree. The capability of DOISST to reconstruct diurnal warming events, which may reach intense amplitudes larger than 5 K in the Mediterranean Sea, is also analysed. Specifically, a comparison with the OSTIA diurnal skin SST product, SEVIRI, model and drifter data, shows that the DOISST product is able to reproduce more accurately diurnal warming events larger than 1 K. This product can contribute to improve the prediction capability of numerical weather forecast systems (e.g., through improved forcing/assimilation), as well as the monitoring of surface heat budget estimates and temperature extremes which can have significant impacts on the marine ecosystem.

30 The full MED DOISST product (released on 04 May 2021) is available upon free registration at
31 https://doi.org/10.25423/CMCC/SST_MED_PHY_SUBSKIN_L4_NRT_010_036 (Pisano et al., 2021). The reduced subset
32 used here for validation and review purposes is openly available at <https://doi.org/10.5281/zenodo.5807729> (Pisano, 2021).
33

34 **1 Introduction**

35 In the last decades, the development of accurate satellite-based Sea Surface Temperature (SST) products required an increasing
36 effort to meet an ever-growing request from scientific, operational and emerging policy needs. Indeed, infrared and/or
37 microwave satellite radiometers allow a systematic and synoptic mapping of the ocean surface temperature (under clear-sky
38 conditions for the infrared and in the absence of rain for the microwave bands) with spatial resolutions from one to few
39 kilometers and temporal sampling from hourly to daily (Minnett et al., 2019). This almost continuous coverage represents a
40 unique characteristic of satellite thermal data, which is clearly not achievable with the use of in situ measurements alone.
41 Indeed, though in situ sensors reach significantly higher accuracy than satellite sensors, with uncertainties that can reach $O(10^2 \text{ K})$, they provide pointwise seawater temperature measurements, generally characterized by a poor and non-uniform sampling
42 of the ocean surface.
43

44 There is a huge variety of satellite-based SST datasets, characterized by different nominal resolutions as well as temporal and
45 spatial (global or regional) coverage, and based on different processing algorithms and satellite sensors, but designed to provide
46 highly accurate SST estimates (Yang et al., 2021). Operational datasets are typically distributed in near real time (NRT),
47 delayed-mode or as reprocessed datasets, and may include different processing levels, from single satellite passes processed
48 to provide valid SST values in the original observation geometry, the so-called Level-2 (L2), to images remapped onto a regular
49 grid, also known as Level-3 (L3), up to the spatially complete Level-4 (L4), interpolated over fixed regular grids. These latter
50 are required by several applications since the lower levels are typically affected by several data voids (due to clouds, rain, land,
51 sea-ice, or other environmental factors depending on the type of sensors). The timely availability of SST data, ranging from a
52 few hours to a few days before real time, allows their use as boundary condition and/or assimilation in meteorological and
53 ocean forecasting systems (Waters et al., 2015), to improve the retrieval of ocean surface currents (Bowen et al., 2002; Rio
54 and Santoleri 2018), and monitor some weather extreme events, such as marine heatwaves (Oliver et al., 2021). The
55 reprocessing of long-term SST data records, typically covering the satellite era (1981-present), aims to provide more stable
56 and consistent datasets, complementing the NRT production, to be used to investigate climate variability and monitor changes
57 from interannual to multi-decadal timescales (Deser et al., 2010), including e.g. SST trends' estimates (Good et al., 2007;
58 Pisano et al., 2020). The Copernicus Marine Environment Monitoring Service (CMEMS) is one of the main examples of how
59 satellite observations, including not only SST but a wide range of surface variables (e.g., sea surface salinity, sea surface

60 height, ocean color, winds and waves), are exploited to derive and disseminate high-level products (Le Traon et al., 2019),
61 namely L4 data in order to be directly usable for downstream applications.

62 The majority of the existing L4 SST datasets are provided as daily, weekly or monthly averaged fields (see e.g. Fiedler et al.,
63 2019; Yang et al., 2021). Examples of well-known state-of-the-art SST daily datasets include the Global Ocean Sea Surface
64 Temperature and Sea Ice (OSTIA) dataset (Good et al., 2020), the European Space Agency (ESA) Climate Change Initiative
65 (CCI), the Copernicus Climate Change Service (C3S) Reprocessed Sea Surface Temperature Analyses (Merchant et al., 2019),
66 and the NOAA Daily Optimally Interpolated SST (OISST) v2.1 dataset, previously known/referred to as Reynolds SST
67 analysis (Huang et al., 2021). Though a daily resolution is generally sufficient to meet the requirements of many of the
68 oceanographic applications, it does not resolve the SST diurnal cycle, the typical day-night SST oscillation mainly driven by
69 solar heating. Within the oceanic thermal skin layer (few μm to 1 mm), SST is typically subject to a large potential diurnal
70 cycle (especially under low wind speed and strong solar heating conditions) reaching amplitudes up to 3 K in the world oceans
71 (Gentemann et al., 2008; Gentemann and Minnett, 2008).

72 The SST diurnal cycle has several implications on mixed layer dynamics, air-sea interaction and the modulation of the lower
73 atmosphere dynamics. The most direct consequence of the SST diurnal amplitude variability is certainly on air-sea fluxes.
74 Clayson and Bogdanoff (2013) estimated that the diurnal SST cycle contributes approximately 5 Wm^{-2} to the global ocean-
75 atmosphere heat budget with peaks of about 10 Wm^{-2} in the Tropics. The inclusion of a realistic diurnal SST cycle in
76 atmospheric numerical simulation also has a non-negligible impact on cloud dynamics. Chen and Houze (1997) have shown
77 that in the Tropical Warm Pool, where extreme localized warming events occur, the diurnal warming can contribute to
78 modulate the evolution of convective clouds and, more in general, can impact the ocean-atmosphere coupling in numerical
79 models, producing a more realistic spatial pattern of warming and precipitation (Bernie et al., 2008). Overall, the diurnal cycle
80 of SST is generally underestimated in current ocean models and the assimilation of SST at high temporal frequency has the
81 potential to improve sea surface variability and mixed layer accuracy (Storto and Oddo, 2019).

82 In principle, the best opportunity to measure the diurnal cycle comes from infrared radiometers on board geostationary
83 satellites. Their observations are sufficiently accurate and frequent to resolve the diurnal signal variability whenever cloud
84 cover is not too persistent. An example is provided by the Spinning Enhanced Visible Infra-Red Imager (SEVIRI) onboard the
85 Meteosat Second Generation (MSG) geostationary satellite covers. The operational retrieval of SST from MSG/SEVIRI
86 (managed by the European Organization for the Exploitation of Meteorological Satellites, EUMETSAT, Ocean and Sea-Ice
87 Facility, OSI-SAF) produces L3C hourly sub-skin SST products by aggregating 15 minutes (MSG/SEVIRI) observations
88 within 1 hour. The sub-skin SST is the temperature at the base of the conductive laminar sub-layer of the ocean surface, as
89 defined by the Group of High Resolution SST (GHRSSST, see e.g. Minnett et al., 2019). In practice, this is the temperature at
90 ~ 1 mm depth (see e.g., [osisaf_cdop3_ss1_pum_msg_sst_data_record.pdf](https://eumetsat.int/Products/osisaf_cdop3_ss1_pum_msg_sst_data_record) (eumetsat.int)), and thus particularly sensitive to
91 diurnal warming.

92 For the global ocean, the Operational Sea surface Temperature and sea Ice Analysis (OSTIA) diurnal product (While et al.,
93 2017) provides daily gap-free maps of hourly mean skin SST at $0.25^\circ \times 0.25^\circ$ horizontal nominal resolution, using in situ and
94 satellite data from infrared radiometers. The skin temperature is defined as the temperature of the ocean measured by an
95 infrared radiometer (typically aboard satellites) and represents the temperature of the ocean within the conductive diffusion-
96 dominated sub-layer at a depth of $\sim 10\text{-}20\ \mu\text{m}$ (GHRSSST, Minnett et al., 2019). This system produces a skin SST by combining
97 the OSTIA foundation SST analysis (Good et al., 2020) with a diurnal warm-layer temperature difference and a cool skin
98 temperature difference derived from numerical models.

99 At regional scale, a method to reconstruct the hourly SST field over the Mediterranean Sea from SEVIRI data has been
100 proposed by Marullo et al. (2014, 2016). The reconstruction is based on a blending of satellite observations and numerical
101 model analyses (used as first-guess) using optimal interpolation. Though model analyses by definition also assimilate
102 observations, which could thus in principle include hourly SEVIRI data, in the present configuration they are not able to deal
103 with such frequent updates (see section 2.2), and the approach presented here represents an effective way to improve the
104 reconstruction of SST daily cycle from high-repetition satellite measurements. Previous works demonstrated the capability of
105 SEVIRI to resolve the SST diurnal variability and to reconstruct accurate L4 SST hourly fields over the Mediterranean Sea, a
106 basin that exhibits large diurnal SST variations (Buongiorno Nardelli et al., 2005; Minnett et al., 2019) that can easily exceed
107 extreme values ($\sim 5\ \text{K}$) as observed in the Tropical Pacific (Chen and Houze 1997), in the Atlantic Ocean and other marginal
108 seas (Gentemann et al., 2008; Merchant et al., 2008). The aim of this paper is to describe the operational implementation of a
109 diurnal optimally interpolated SST (DOISST) product for the Mediterranean Sea (MED), building on the algorithm by Marullo
110 et al. (2014, 2016). The DOISST product routinely provides hourly mean maps of sub-skin SST at $1/16^\circ$ horizontal resolution
111 over the Mediterranean Sea from January 2019 to present. The assessment presented here for the DOISST product covers two
112 complete years (2019-2020), thus extending previous similar validations (Marullo et al., 2016).

113

114 **2 The data**

115 **2.1 Satellite data**

116 Input satellite SST is derived from the SEVIRI sensor onboard the Meteosat Second Generation (Meteosat-11) satellite.
117 SEVIRI has a repeat cycle of 15 minutes over the $60\text{S-}60\text{N}$ and $60\text{W-}60\text{E}$ domain: Atlantic Ocean, European Seas and western
118 Indian Ocean. The retrieval of SST from Meteosat-11/SEVIRI is managed by EUMETSAT OSI-SAF, which provides sub-
119 skin SST data as aggregated (L3C) hourly products remapped onto a 0.05° regular grid. Hourly products result from
120 compositing the best SST measurements available in one hour and are made available in near real time with a timeliness of 3
121 hours (see the OSI-SAF product user manual, <https://osi-saf.eumetsat.int/products/osi-206>). File format follows the Data

122 Specification (GDS) version 2 from the Group for High Resolution Sea Surface Temperatures (GHRSSST, [https://podaac-](https://podaac-tools.jpl.nasa.gov/drive/files/OceanTemperature/ghrsst/docs/GDS20r5.pdf)
123 [tools.jpl.nasa.gov/drive/files/OceanTemperature/ghrsst/docs/GDS20r5.pdf](https://podaac-tools.jpl.nasa.gov/drive/files/OceanTemperature/ghrsst/docs/GDS20r5.pdf)). The computation of SST in day and night
124 conditions is based on a nonlinear split window algorithm whose coefficients are determined from brightness temperature
125 simulations on a radiosonde profile database, with an offset coefficient corrected relative to buoy measurements. A correction
126 term derived from simulated brightness temperatures with an atmospheric radiative transfer model is then applied to the
127 multispectral derived SST (OSI-SAF PUM, https://osi-saf.eumetsat.int/lml/doc/osisaf_cdop3_ss1_pum_geo_sst.pdf). L3C
128 data are provided with additional information, including quality level and cloud flags. Such quality flags are provided at pixel
129 level, ranging over a scale of five levels with increasing reliability: 1 (=“cloudy”), 2 (=“bad”), 3 (=“acceptable”), 4 (=“good”)
130 to 5 (=“excellent”).

131 The accuracy of Meteosat-11 SST data has been assessed through comparison with co-located drifting buoys, for day and
132 night data separately covering the period from February to June 2018 (see the OSI-SAF scientific validation report, [https://osi-](https://osi-saf.eumetsat.int/lml/doc/osisaf_cdop2_ss1_geo_sst_val_rep.pdf)
133 [saf.eumetsat.int/lml/doc/osisaf_cdop2_ss1_geo_sst_val_rep.pdf](https://osi-saf.eumetsat.int/lml/doc/osisaf_cdop2_ss1_geo_sst_val_rep.pdf)). The mean bias and standard deviation (derived from the
134 differences between SEVIRI SSTs and drifter measurements over a matchup database) during nighttime have been quantified
135 in -0.1 K and 0.53 K, respectively. During daytime, the bias remains practically unchanged (-0.09 K) and the standard deviation
136 slightly higher (0.56 K). These statistics were derived by selecting SEVIRI SST with quality flags ≥ 3 , and it is shown that the
137 quality of SST improves when choosing higher quality levels. A similar validation procedure (Marullo et al., 2016), but
138 performed over the Mediterranean Sea by using nighttime and daytime data selected with quality flags ≥ 4 , shows that SEVIRI
139 SST bias and standard deviation are -0.03 K and 0.47 K, respectively.

140 For our purposes, we selected L3C SST data with quality flag ≥ 3 , as also indicated/suggested in the OSI-SAF scientific
141 validation report. A synthesis of the SEVIRI SST characteristics is reported in Table 1.

142 **2.2 Model data**

143 The model output fields of surface temperature are derived from the CMEMS Mediterranean Sea Physical Analysis and
144 Forecasting product, and identified as MEDSEA_ANALYSIS_FORECAST_PHY_006_013
145 ([https://resources.marine.copernicus.eu/product-](https://resources.marine.copernicus.eu/product-detail/MEDSEA_ANALYSISFORECAST_PHY_006_013/INFORMATION)
146 [detail/MEDSEA_ANALYSISFORECAST_PHY_006_013/INFORMATION](https://resources.marine.copernicus.eu/product-detail/MEDSEA_ANALYSISFORECAST_PHY_006_013/INFORMATION);
147 https://doi.org/10.25423/CMCC/MEDSEA_ANALYSISFORECAST_PHY_006_013_EAS6; last access: 03 November 2021;
148 Clementi et al., 2021), and routinely produced by the CMEMS Mediterranean Monitoring and Forecasting Center (Med-MFC).
149 The modelling system is based on the Mediterranean Forecasting System, MFS (Pinardi et al., 2003), a coupled hydrodynamic-
150 wave model implemented over the Mediterranean basin, extended into the Atlantic Sea in order to better resolve the exchanges
151 with the Atlantic Ocean at the Strait of Gibraltar, with a horizontal grid resolution of $1/24^\circ$ (~ 4 km) and 141 unevenly spaced
152 vertical levels (Clementi et al., 2017). The Ocean General Circulation Model is based on the Nucleus for European Modelling
153 of the Ocean (NEMO v3.6) (Oddo et al., 2014, 2009), while the wave component is provided by Wave Watch-III. The model

154 solutions are corrected by a variational data assimilation scheme (3DVAR) of temperature and salinity vertical profiles and
155 along track satellite sea level anomaly observations (Dobricic and Pinardi 2008). The CMEMS Mediterranean SST L4 product
156 (CMEMS product reference: SST_MED_SST_L4_NRT_OBSERVATIONS_010_004,
157 [https://resources.marine.copernicus.eu/product-
158 detail/SST_MED_SST_L4_NRT_OBSERVATIONS_010_004/INFORMATION](https://resources.marine.copernicus.eu/product-detail/SST_MED_SST_L4_NRT_OBSERVATIONS_010_004/INFORMATION); last access: 03 November 2021) is used for
159 the correction of surface heat fluxes with the relaxation constant of $110 \text{ Wm}^{-2}\text{K}^{-1}$ centered at midnight since the product
160 provides foundation SST (~SST at midnight).

161 The Med-MFC product is produced with two different cycles: a daily cycle for the production of forecasts (i.e., ten-days
162 forecast on a daily basis), and a weekly cycle for the production of analyses. For our purposes, only hourly mean fields of sea
163 surface temperature, which correspond to the first vertical level of the model centered at ~1 m from the surface, are selected.
164 A synthesis of the model-derived SST characteristics is reported in Table 1.

165 **2.3 In situ data**

166 Surface drifting buoys have been used for validation purposes (Section 4). Since there are no in situ instruments able to
167 routinely measure skin/sub-skin SSTs, the commonly adopted validation procedure is to use drifters' data, also due to their
168 high accuracy and closeness to the sea surface (their representative depth attains around ~20 cm; Reverdin et al., 2010), and
169 to their abundance compared to other in situ instruments, which allows to achieve a more consistent and homogeneous temporal
170 and spatial coverage. Of course, these observations are affected by a representativeness error when compared to sub-skin SSTs,
171 which is typically quantified in terms of a bias between the two estimates.

172 Drifter data have been obtained from the CMEMS IN SITU (INS) TAC (identified as
173 INSITU_MED_NRT_OBSERVATIONS_013_035, [https://resources.marine.copernicus.eu/product-
174 detail/INSITU_MED_NRT_OBSERVATIONS_013_035/INFORMATION](https://resources.marine.copernicus.eu/product-detail/INSITU_MED_NRT_OBSERVATIONS_013_035/INFORMATION); and
175 INSITU_IBI_NRT_OBSERVATIONS_013_033, [https://resources.marine.copernicus.eu/product-
176 detail/INSITU_IBI_NRT_OBSERVATIONS_013_033/INFORMATION](https://resources.marine.copernicus.eu/product-detail/INSITU_IBI_NRT_OBSERVATIONS_013_033/INFORMATION); last access: 03 November 2021), which collects
177 and distributes a variety of physical and biogeochemical seawater measurements, provided with the same homogeneous file
178 format. Each in situ measurement, including drifters, undergoes automated quality controls before its distribution. The quality
179 of the data is expressed by control flags indexed from 0 to 9, with the value of 1 indicating best quality. Drifter data have been
180 used to compile an hourly matchup database of co-located (in space and time) diurnal optimally interpolated SST (DOISST)
181 values and model outputs (Section 4.1), and validation statistics are based on the comparison among DOISST, model SST and
182 drifting buoy measurements over the matchup database (Section 4.2). A synthesis of the drifter SST characteristics is reported
183 in Table 1.

184 **2.4 OSTIA diurnal**

185 The OSTIA diurnal skin SST product (While et al., 2017) provides gap-free global maps of hourly mean skin SST at 0.25° x
186 0.25° horizontal resolution, obtained by combining in situ and infrared satellite data. This product is operationally produced
187 by the Met Office within the Copernicus Marine Service (identified as
188 SST_GLO_SST_L4_NRT_OBSERVATIONS_010_014, [https://resources.marine.copernicus.eu/product-](https://resources.marine.copernicus.eu/product-detail/SST_GLO_SST_L4_NRT_OBSERVATIONS_010_014/INFORMATION)
189 detail/SST_GLO_SST_L4_NRT_OBSERVATIONS_010_014/INFORMATION; last access: 02 May 2022), and created
190 using the Operational Sea surface Temperature and Ice Analysis (OSTIA) system (Good et al., 2020). The OSTIA system also
191 produces a global daily average foundation SST L4 product (identified as
192 SST_GLO_SST_L4_NRT_OBSERVATIONS_010_001, [https://resources.marine.copernicus.eu/product-](https://resources.marine.copernicus.eu/product-detail/SST_GLO_SST_L4_NRT_OBSERVATIONS_010_001/INFORMATION)
193 detail/SST_GLO_SST_L4_NRT_OBSERVATIONS_010_001/INFORMATION; last access: 02 May 2022). Since the skin
194 SST can be considered as the sum of three components, namely the foundation SST, the warm layer and the cool skin, the
195 OSTIA diurnal product is created by adjusting the OSTIA foundation SST analysis with a modelled diurnal warm layer analysis
196 (which assimilates satellite observations) and a cool skin model, based respectively on the Takaya (Takaya et al., 2010) and
197 Artale models (Artale et al., 2002). Assimilation into the warm layer model makes use of SEVIRI, GOES-W and MTSAT-2
198 geostationary infrared sensors, and of the polar orbiting VIIRS radiometer. Further details on the method can also be found in
199 Copernicus PUM (<https://catalogue.marine.copernicus.eu/documents/PUM/CMEMS-SST-PUM-010-014.pdf>). A synthesis of
200 the OSTIA diurnal SST characteristics is reported in Table 1.

201
202
203
204
205
206
207
208
209
210
211
212
213
214
215
216

SST							
Source	Definition	Vertical level	Spatial res.	Temporal res.	Spatial coverage	Temporal coverage	Processing level
Model	Depth SST	1 m (first model layer)	0.042°x0.042°	Hourly	17.3°W–36.3°E, 30.2°N–46°N	2019-Present	Model output
SEVIRI	Sub-skin SST	~1 mm (surface only)	0.05°x0.05°	Hourly	60°W–60°E, 60°S–60°N	2015-Present	L3C
OSTIA diurnal	Skin SST	~10-20 μm (surface only)	0.25°x0.25°	Hourly	Global	2015-Present	L4
Surface Drifting Buoys	Depth SST	~20 cm (surface only)	Not applicable	Hourly	30°W–36.5°E, 20°N–55°N	2010-Present	L2

217

218

219

220

221

222

Table 1. Summary of the SST products used to produce (Model and SEVIRI), validate (surface drifting buoys), and intercompare (all) the DOISST product. The SST nomenclature (skin, sub-skin, and depth) follows the Group for High Resolution Sea Surface Temperatures (GHRSSST) definitions (<https://podaac-tools.jpl.nasa.gov/drive/files/OceanTemperature/ghrsst/docs/GDS20r5.pdf>).

223

3 The Mediterranean diurnal optimally interpolated SST product

224

3.1 Product overview

225

226

227

228

229

230

231

232

233

234

235

236

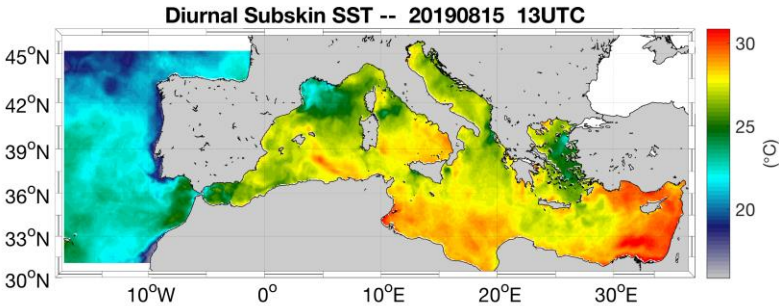
The Mediterranean diurnal optimally interpolated SST (hereafter referred to as MED DOISST) operational product consists of hourly mean gap-free (L4) satellite-based estimates of the sub-skin SST over the Mediterranean Sea (plus the adjacent Eastern Atlantic box, see Section 2.2) at 0.0625° x 0.0625° grid resolution, from 1st January 2019 to near real time. Specifically, the product is updated daily and provides 24 hourly mean data of the previous day, centered at 00:00, 01:00, 02:00,...,23:00 UTC. The MED DOISST product is published on the CMEMS on line catalogue and identified as SST_MED_PHY_SUBSKIN_L4_NRT_010_036 (CMEMS product reference) and cmems_obs-sst_med_phy-sst_nrt_diurnal-oi-0.0625deg_PT1H-m (CMEMS dataset reference). Further details on the product characteristics are provided in Table 2.

DOISST is the result of a blending of sub-skin SSTs and modelled SSTs (as detailed in the next section), the former representative of a depth of 1 mm and the latter of 1 m. Then, the DOISST effective depth does, in principle, vary between 1 mm up to 1 m, depending on how many satellite observations enter the interpolation. As diurnal warming is significantly reduced under cloudy conditions, however, the difference between the SST at 1 m and the sub-skin SST will be much smaller

237 when SEVIRI observations are not present. For this reason, we can define the DOISST product as representative of sub-skin
 238 values.
 239

CMEMS Product ID: SST_MED_PHY_SUBSKIN_L4_NRT_010_036

CMEMS Dataset ID: cmems_obs-sst_med_phy-sst_nrt_diurnal-oi-0.0625deg_PT1H-m

General description	<p>The CMEMS Mediterranean diurnal product provides near-real-time, hourly mean, gap-free (L4) sub-skin SST fields over the Mediterranean Sea and the adjacent Atlantic box over a 0.0625°x0.0625° regular grid, covering the period from 2019 to present (one day before real time). This product is built from optimal interpolating the Level-3C (merged single-sensor, L3C) SEVIRI data as observations and the CMEMS Mediterranean model analyses as first-guess.</p>
	
Horizontal resolution	0.0625° x 0.0625° (1/16°) degrees [871x253]
Temporal resolution	Hourly
Spatial coverage	Mediterranean Sea + adjacent North Atlantic box (W=-18.1250, E=36.2500, S=30.2500, N=46.0000)
Temporal coverage	2019/01/01 – near real time (-14H)
Vertical level	~1 mm (surface only)
Variables	Sub-skin SST (K) Analysis Error (%)
Format	NetCDF – CF-1.4 convention compliant
DOI	https://doi.org/10.25423/CMCC/SST_MED_PHY_SUBSKIN_L4_NRT_010_036
Comments	Eventual updates of this product will be described in the corresponding Product User Manual (PUM) and Quality Information Document (QUID) available on the CMEMS on line catalogue.

240
 241 **Table 2.** The CMEMS MED DOISST product description synthesis.

242 **3.2 Background**

243 The reconstruction of gap-free hourly mean SST fields is based on a blending of satellite observations and model analyses
244 (used as first-guess/background) using optimal interpolation (OI), following the approach proposed by Marullo et al. (2014).
245 The OI method determines the optimal solution to the interpolation of a spatially and temporally variable field with data voids,
246 where “optimal” is intended in a least square sense (see e.g. Bretherton et al., 1976). The optimally interpolated variable, or
247 analysis (F_a), is obtained as follows:

$$248 \quad F_a(x, t) = F_b(x, t) + \sum_{i,j=1}^n W_{i,j} (F_{obs,i}(x, t) - F_b(x, t)) \quad (1)$$

250
251 In practice, the analysis $F_a(x, t)$ at a particular location in space and time (x, t) is obtained as a correction to a background
252 field ($F_b(x, t)$). The correction is estimated as a linear combination of the observation anomalies ($F_{obs} - F_b$), where the
253 coefficients $W_{i,j}$ are obtained by minimizing the analysis error variance.

254 The choice of using a model output as first-guess represents the best alternative to the use of climatologies or previous analyses,
255 as usually done by other schemes to produce daily SST L4 maps, since the model provides physically consistent estimates of
256 hourly SSTs in the absence of any observation or in situ measurement (Marullo et al., 2014). In fact, the model takes into
257 account the effect of air-sea interactions by imposing external forcings that drive momentum and heat exchanges at the upper
258 boundary. As such, it is able to reproduce at least part of the diurnal warming effects, that are driven by the forcing diagnosed
259 from atmospheric model analyses. Using the model output as a first-guess means we are treating the hourly satellite data as
260 corrections to the hourly model data. These anomalies are generally small and mostly drive corrections to the spatial patterns,
261 while displaying a reduced diurnal cycle. Anomaly data from different times of the day can thus be more “safely” used to build
262 the interpolated field at each reference time (with different weights). Unfortunately, the first model layer is at 1 m depth, which
263 means that it will generally underestimate the diurnal cycle anyway. While 1D models could in principle be used to better
264 reproduce sub-skin SST from model data, the approach presented here is focusing on providing estimates that are as close as
265 possible to the original satellite data, avoiding the complications of setting up an additional preprocessing step just to improve
266 the first-guess.

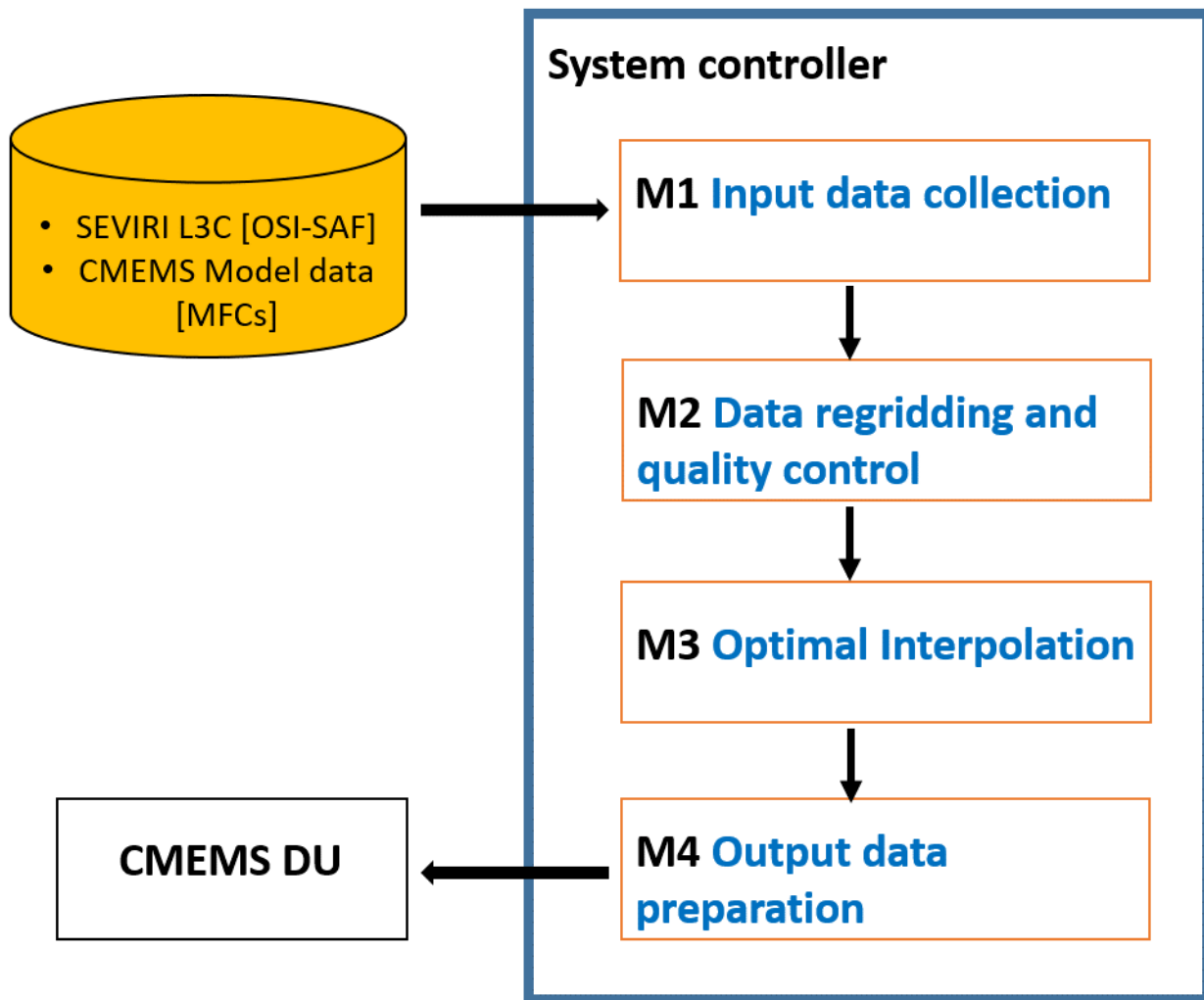
267

268 **3.3 Processing chain**

269 The DOISST system ingests merged single-sensor (L3C) SEVIRI data as the observation source, and the CMEMS
270 Mediterranean Sea model outputs (first layer) as first-guess.

271 The data sub-sampling strategy, inversion technique and numerical implementation of the optimal interpolation scheme are
272 based on the CMEMS NRT MED SST processing chain (Buongiorno Nardelli et al., 2013), which provides daily mean fields

273 of foundation SST over the Mediterranean Sea (CMEMS product reference:
274 SST_MED_SST_L4_NRT_OBSERVATIONS_010_004, [https://resources.marine.copernicus.eu/product-
275 detail/SST_MED_SST_L4_NRT_OBSERVATIONS_010_004/INFORMATION](https://resources.marine.copernicus.eu/product-detail/SST_MED_SST_L4_NRT_OBSERVATIONS_010_004/INFORMATION); last access: 03 November 2021). Here, the
276 diurnal SST chain is organized in three main modules (Fig. 1).



277
278 **Figure 1.** Schematic diagram of the processing chain used for the MED DOISST SST product.
279

280 Module M1 manages the external interfaces to get both upstream L3C SST and model data: hourly mean L3C sub-skin SST
281 data at 0.05° grid resolution are downloaded from OSI-SAF; hourly seawater potential temperatures at 1.0182 meter are
282 obtained from the CMEMS Mediterranean Sea model outputs, provided on a 0.042° regular grid.

283 Module M2 extracts and regrids (through bilinear interpolation) L3C data and model outputs over the CMEMS Mediterranean
284 Sea geographical area (see Table 2). A selection over SEVIRI is performed by flagging the pixels with quality flag < 3.

285 Module M3 performs a space-time optimal interpolation (OI) algorithm. L4 data are obtained as a linear combination of the
286 SST anomalies, weighted directly with their correlation to the interpolation point and inversely with their cross-correlation and
287 error (Eq. 1). Correlations are typically expressed through analytical functions with predefined spatial and temporal de-
288 correlation lengths. Here, the covariance function $f(r, \Delta t)$ is the one defined in Marullo et al. (2014), and given as the product
289 of a spatial and temporal component:

$$290 \quad f(r, \Delta t) = \left[\alpha \cdot e^{-\frac{r}{R}} + \frac{1-\alpha}{(1+r)^c} \right] \cdot e^{-\left(\frac{\Delta t}{T}\right)^d} \quad (2)$$

291

292 where r is the distance (in km) between the observation and the interpolation point; Δt is the temporal difference (in hours)
293 between the observation and the interpolation point; $R = 200$ km is the decorrelation spatial length; $T = 36$ h is the decorrelation
294 time length; the other parameters are set as follows: $a = 0.70$, $c = 0.26$, $d = 0.4$. All these parameters have been derived in
295 Marullo et al. (2014), deduced from a nonlinear least square fit between the estimated temporal and spatial correlations. In
296 practice, the weights in expression (1) are computed directly from the analytical function (2).

297 The input data are selected only within a limited sub-domain (within a given space-time interval, also called “influential”
298 radius), with a temporal window of ± 24 h (this is the result of several trials over a large variety of environmental conditions;
299 Marullo et al., 2014) and a spatial search radius of about 700 km (Buongiorno Nardelli et al., 2013). A check to avoid data
300 propagation across land is performed between each pixel within the sub-domain and the given interpolation point (eventually
301 discarded if there are land pixels between the straight line connecting the two points).

302 The interpolation error (analysis_error field in the L4 file, Table 2) is obtained from the formal definition of the error variance
303 derived from optimal interpolation theory (e.g., Bretherton et al., 1976). This error ranges between 0-100%, meaning that the
304 error is almost zero when an optimal number of observations is present within the space-time influential radius, while only
305 first-guess data are used (i.e. no observations are found within the search radius) when the error is 100%.

306 The optimal interpolation algorithm is synthesized as follows:

- 307 • Hourly SEVIRI and model SSTs in a space/time window of 700 km/ ± 24 h around the interpolation position/time are
308 ingested;
- 309 • SEVIRI data with quality flag ≥ 3 are retained;
- 310 • Regridding over the Mediterranean Sea;
- 311 • Hourly model SSTs are subtracted from valid SSTs producing SST anomalies;

- SST anomalies are used as data input for the optimal interpolation analysis;
- Optimal interpolation is run using the covariance function defined above;
- The model SST is added to the optimally interpolated output again.

The only difference with the original method is that all the input observations are interpolated, while in Marullo et al. (2014) valid SST observations are left unchanged (not interpolated).

4 Validation of diurnal product

4.1 Validation framework

The accuracy of the MED DOISST product has been assessed through comparison with independent co-located (in space and time) surface drifting buoy data (matchups). The validation framework is based on the compilation of a matchup database between DOISST and drifters measurements covering the full years 2019 and 2020. The large number of drifters provides a rather homogeneous and continuous spatial and temporal coverage over the whole period (Fig. 2) allowing a robust statistical approach.

Firstly, a pre-selection of high-quality drifter data is performed, retaining only temperatures with quality flag equal to 1 (good) or 2 (probably good) (see section 2.3). Then, the co-location is carried out on hourly basis, building a matchup database by collecting the closest (in space) SST grid point to the in situ measurement within a symmetric temporal window of 30 minutes with respect to the beginning of each hour. A final quality outlier detection check is carried out by identifying drifter data for which the module of the difference with respect to satellite observations exceeds n -times the standard deviation σ of the distribution of the differences (δ). At each step n decreases, and data that fall out of the interval $I = [mean(\delta) - n \cdot \sigma, mean(\delta) + n \cdot \sigma]$ are flagged as outliers and removed. For each n , the selected outliers are eliminated and the process is repeated for the same value of n until no more outliers are detected. Then the system moves to $n-1$. The process starts for $n=10$ and stops at $n=3$, and removes $\sim 1\%$ of the total original sampling (as expected from a gaussian distribution) of drifter data that clearly revealed anomalous temperature values.

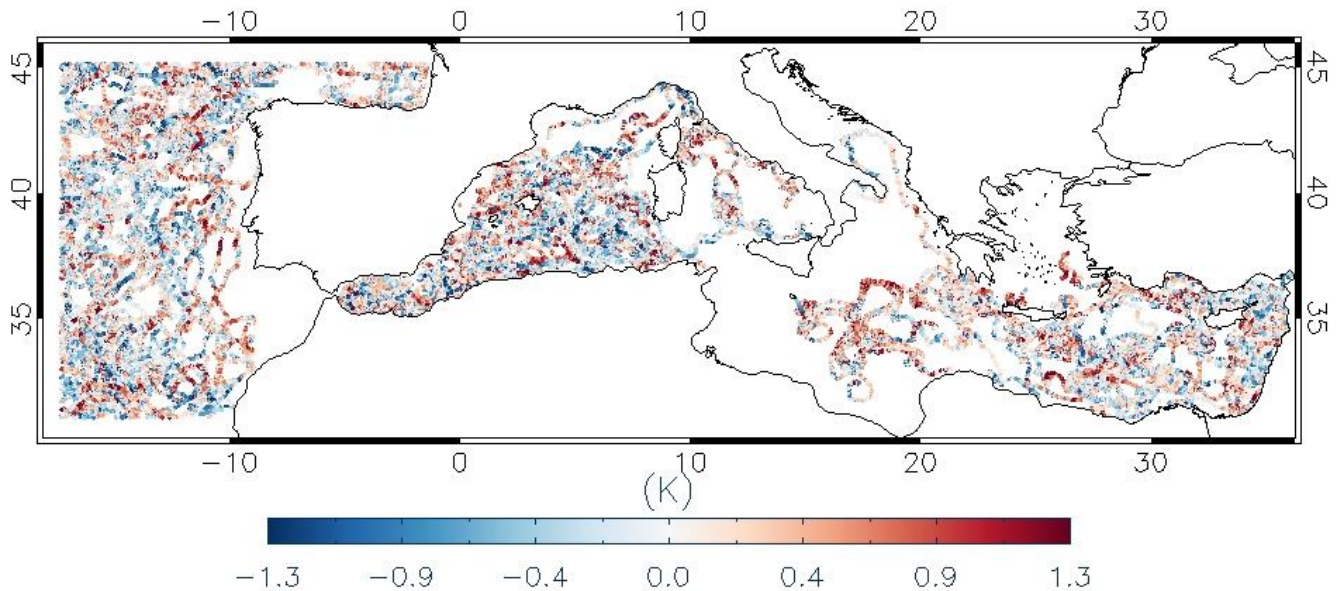
The main validation statistics are quantified in terms of mean bias and Root-Mean-Square Difference (RMSD) from matchup temperature differences (namely, SST minus drifter). Each statistical parameter is associated with a 95% confidence interval computed through a bootstrap procedure (Efron 1994).

In order to evaluate the DOISST performance with respect to the model, the same validation procedure has been applied to the modelled SST.

341 **4.2 Comparison with drifters**

342 **4.2.1 The mean diurnal cycle**

343 The spatial distribution of DOISST and drifter matchups over the 2019-2020 period, along with their pointwise difference (i.e.,
344 DOISST minus drifter measurement) shows a rather homogeneous coverage over the most of the CMEMS MED domain (Fig.
345 2), although some areas are characterized by quite low coverage, such as the North Adriatic Sea or North Aegean Sea. The
346 spatial distribution also evidences the predominance of a positive bias, indicating that DOISSTs are warmer than drifters'
347 temperatures on average.



348 **Figure 2.** Spatial distribution of the matchup points along with their punctual bias (i.e., SST minus drifter data, K) over the
349 CMEMS Mediterranean domain from 2019/01/01 to 2020/12/31.
350

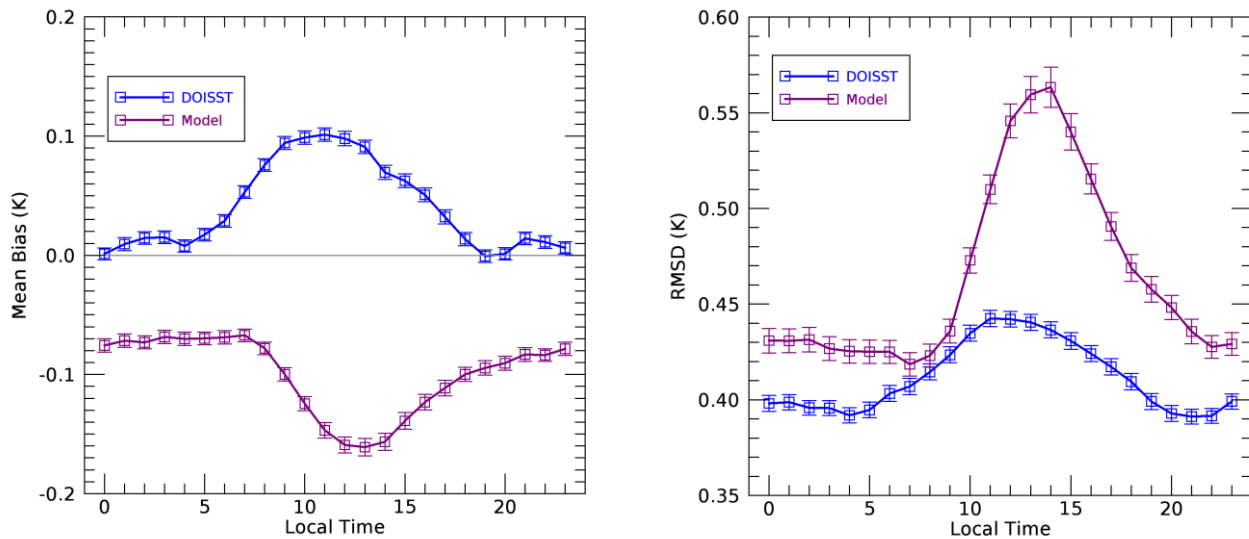
351
352
353 The DOISST product shows effectively an overall small positive mean bias of 0.041 ± 0.001 K and a RMSD of 0.412 ± 0.001
354 K (Table 2). A negative bias of -0.100 ± 0.001 K and slightly larger RMSD of 0.467 ± 0.001 K characterize model SSTs. Both
355 DOISST and the model show high and comparable correlation coefficients (more than 0.99).
356

357
358
359
360
361

	Period	Mean bias (K)	RMSD (K)	Correlation coeff.	Matchups
DOISST	2019-01-01 to 2020-12-31	0.041 ± 0.001	0.412 ± 0.001	0.992	548959
Model	2019-01-01 to 2020-12-31	-0.100 ± 0.001	0.467 ± 0.001	0.991	548959

362 **Table 3.** Summary statistics of DOISST and model outputs. Mean bias (K), RMSD (K), and correlation coefficient are derived
363 from temperature differences against drifters' data over the period 2019-2020. Each statistical parameter is associated with a
364 95% confidence interval computed through a bootstrap procedure (Efron 1994).

365
366 The hourly mean bias of DOISST and model shows similar but opposite behaviour (Fig. 3, and Table 4). In both cases, the
367 bias clearly exhibits a diurnal oscillation during the 24 hours but, while the bias of DOISST increases positively during the
368 central diurnal warming hours, the one of the model increases negatively. The DOISST mean bias is practically null between
369 17:00 to 06:00 local time, ranging between -0.001 and 0.03 K, and highest (~ 0.1 K) between 10:00 and 13:00 local time. The
370 bias of the model oscillates around ~ -0.07 K between 23:00 and 07:00 local time. Then, it increases (in absolute value) reaching
371 the peak of ~ -0.16 K between 11:00 and 14:00 and decreases successively. Similar results are obtained for the RMSD, which
372 increases with diurnal warming (Fig. 3, Table 4). However, the RMSD of DOISST is less impacted by diurnal variations,
373 characterized by an amplitude of ~ 0.04 K against ~ 0.14 K of the model.



374 **Figure 3.** Mean bias (K) and RMSD (K) relative to MED DOISST (blue line) and model (purple line) based on the differences
375 against drifters' data. Mean bias and RMSD are given as hourly mean over the period 2019-2020.

Hour (local time)	Mean BIAS (K) (DOISST)	RMSD (K) (DOISST)	BUOY-AVAIL	Mean BIAS (K) (Model)	RMSD (K) (Model)
HH: 00	0.001 ± 0.005	0.398 ± 0.004	22807	-0.076 ± 0.006	0.431 ± 0.006
HH: 01	0.009 ± 0.005	0.399 ± 0.004	23004	-0.072 ± 0.006	0.431 ± 0.006
HH: 02	0.014 ± 0.005	0.396 ± 0.004	22798	-0.073 ± 0.005	0.431 ± 0.006
HH: 03	0.015 ± 0.005	0.396 ± 0.004	23078	-0.068 ± 0.006	0.427 ± 0.006
HH: 04	0.008 ± 0.005	0.392 ± 0.004	22857	-0.070 ± 0.005	0.425 ± 0.006
HH: 05	0.017 ± 0.005	0.395 ± 0.004	22806	-0.070 ± 0.005	0.425 ± 0.006
HH: 06	0.029 ± 0.005	0.403 ± 0.004	22819	-0.069 ± 0.006	0.425 ± 0.006
HH: 07	0.053 ± 0.005	0.407 ± 0.004	23379	-0.067 ± 0.005	0.419 ± 0.006
HH: 08	0.076 ± 0.005	0.415 ± 0.004	23501	-0.078 ± 0.006	0.423 ± 0.006
HH: 09	0.094 ± 0.005	0.423 ± 0.004	23481	-0.100 ± 0.006	0.436 ± 0.006
HH: 10	0.099 ± 0.006	0.435 ± 0.004	23270	-0.125 ± 0.006	0.473 ± 0.007
HH: 11	0.101 ± 0.006	0.442 ± 0.004	23311	-0.147 ± 0.006	0.510 ± 0.007
HH: 12	0.098 ± 0.006	0.442 ± 0.004	23129	-0.159 ± 0.007	0.546 ± 0.009
HH: 13	0.091 ± 0.006	0.440 ± 0.005	22836	-0.161 ± 0.007	0.560 ± 0.009
HH: 14	0.070 ± 0.006	0.436 ± 0.004	22673	-0.157 ± 0.007	0.563 ± 0.011
HH: 15	0.062 ± 0.006	0.431 ± 0.004	22418	-0.139 ± 0.007	0.540 ± 0.009
HH: 16	0.051 ± 0.006	0.424 ± 0.004	22368	-0.123 ± 0.007	0.515 ± 0.008
HH: 17	0.032 ± 0.006	0.417 ± 0.004	22019	-0.111 ± 0.006	0.491 ± 0.007
HH: 18	0.014 ± 0.006	0.410 ± 0.004	21916	-0.100 ± 0.006	0.469 ± 0.007
HH: 19	-0.001 ± 0.005	0.399 ± 0.004	22117	-0.095 ± 0.006	0.458 ± 0.007
HH: 20	0.001 ± 0.005	0.393 ± 0.004	22458	-0.090 ± 0.006	0.448 ± 0.006
HH: 21	0.014 ± 0.005	0.391 ± 0.004	23229	-0.083 ± 0.005	0.436 ± 0.006
HH: 22	0.011 ± 0.005	0.392 ± 0.004	23272	-0.084 ± 0.006	0.428 ± 0.006
HH: 23	0.006 ± 0.005	0.399 ± 0.004	23413	-0.078 ± 0.006	0.429 ± 0.006

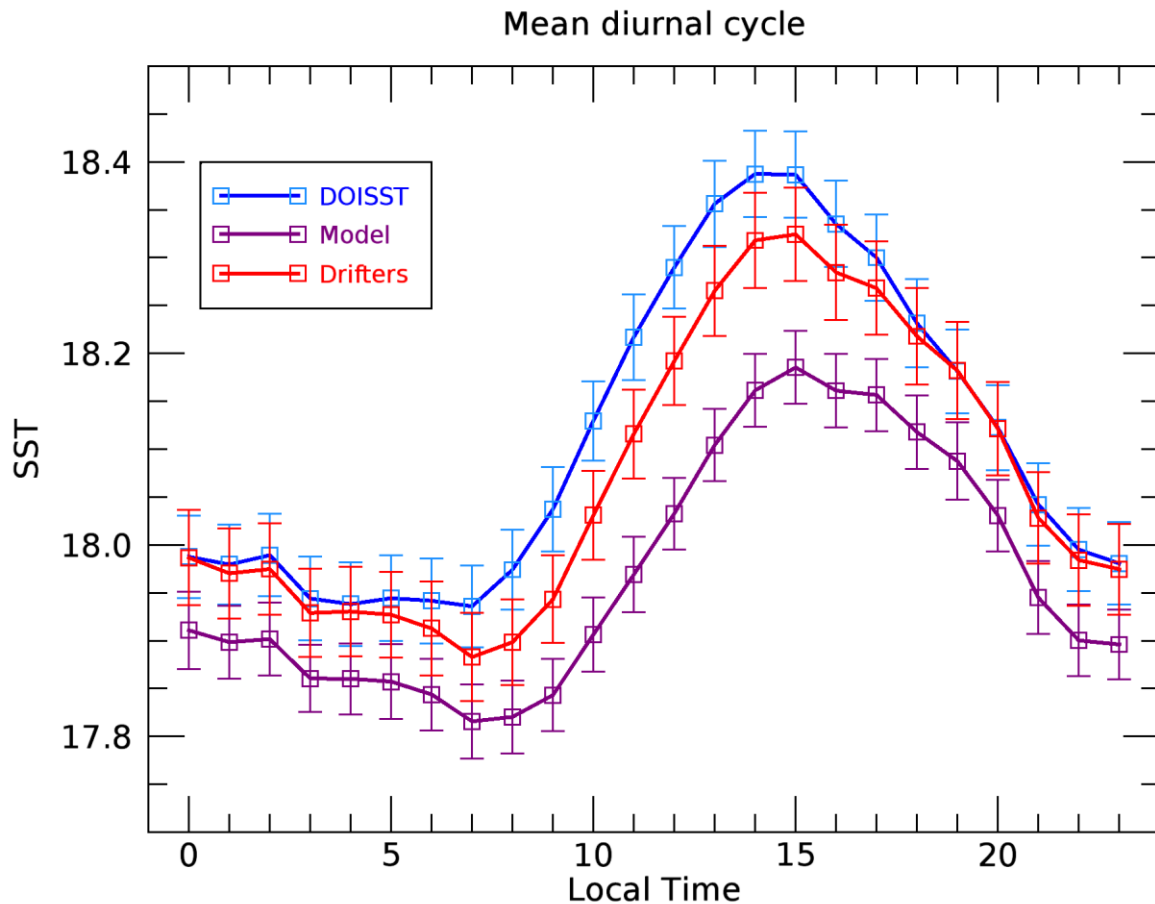
376

377 **Table 4.** Summary statistics of MED DOISST and model products based on the differences against drifters' data over the
378 matchup points. Mean bias (K), RMSD (K) and number of matchups are given as hourly mean over the period 2019-2020.
379 Each statistical parameter is associated with a 95% confidence interval computed through a bootstrap procedure (Efron 1994).

380

381 The mean diurnal cycle of DOISST (namely, the 24-hour mean SSTs estimated over the matchup dataset) is in very good
382 agreement, within the error confidence interval, with the SST cycle reconstructed from drifters (Fig. 4). The two diurnal cycles
383 are practically unbiased between 17:00 and 06:00, while they are biased by ~0.1 K between sunrise and 16:00, coherently with
384 the DOISST bias oscillation (Fig. 3). This bias could be related to skin SST getting warmer faster than the temperature at 20
385 cm depth. The diurnal cycle of model SST maintains always below that of in situ temperatures, evidencing larger differences

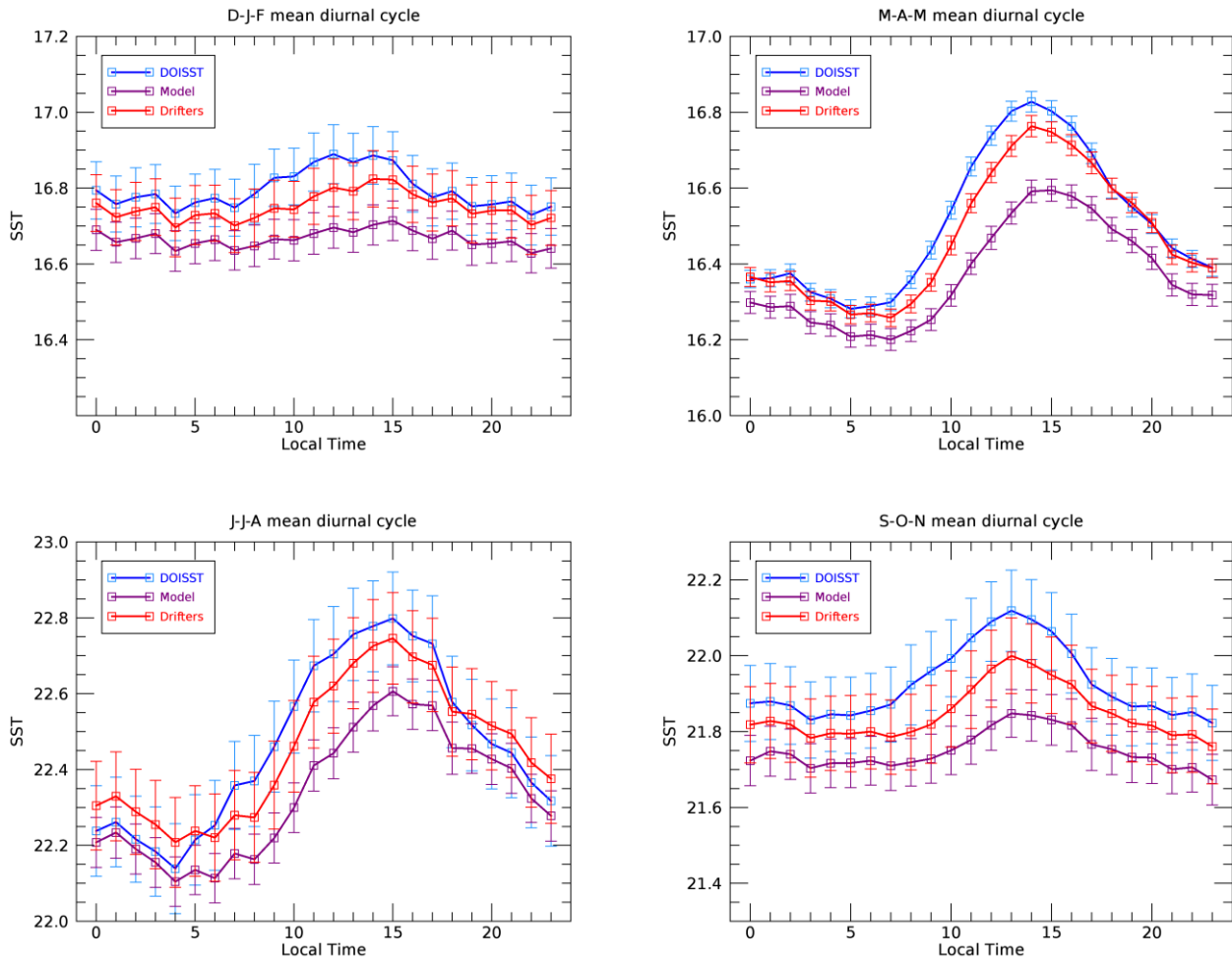
386 during the central diurnal warming hours (Fig. 4). However, apart from the biases likely induced by the different depths, the
387 SST amplitude as estimated from the DOISST and the model is $\sim 2.3\%$ larger and $\sim 16\%$ smaller than that of drifters,
388 respectively, suggesting that the model tends to underestimate diurnal variations.



389
390 **Figure 4.** Mean diurnal cycle for MED DOISST (blue line), model (purple line) and drifters (red line) computed over the
391 matchups from 2019 to 2020.
392

393 A delay of ~ 1 hour of the model with respect to DOISST and in situ on the onset of diurnal warming and in reaching the
394 maximum is also evident. This delay could be explained as the physical result of delayed solar heating of the skin layer sensed
395 by the satellite and of the first model layer. This may also be a consequence of the different packaging of the SEVIRI and
396 model SST data into the hourly files: model hourly SST fields are centered at half of every hour (e.g., 12:30), while SEVIRI
397 L3C at the beginning of each hour (e.g., 12:00) and obtained from collating data within one hour (from 11:30 to 12:29).

398 The capability of DOISST to capture and realistically reproduce diurnal variability is further investigated by analysing the
 399 seasonally averaged SST diurnal cycle (Fig. 5), computed as for the mean diurnal cycle (by using the matchup dataset) but
 400 over seasons: winter (December to February, D-J-F), spring (March to May, M-A-M), summer (June to August, J-J-A) and
 401 autumn (September to November, S-O-N). The effect of warming in the diurnal SST excursion is clearly more pronounced
 402 during spring and summer than winter and autumn, and reconstructed well in DOISST. During the warmer seasons, the
 403 DOISST shows the lower biases (Table 5), estimated in 0.036 ± 0.001 K (spring) and 0.012 ± 0.003 (summer). Conversely,
 404 the model reaches its higher biases, namely -0.101 ± 0.001 K (spring) and -0.117 ± 0.003 K (summer). The good agreement
 405 between DOISST and drifters during winter and autumn (Table 5) reveals that the hourly DOISST fields are reconstructed
 406 accurately also under cloudy conditions, which are more frequent during these seasons (Kotsias and Lolis, 2018).



407
 408 **Figure 5.** Seasonal mean diurnal cycle over the period 2019-2020 for MED DOISST (blue line), model (purple line) in situ
 409 (red line).

	Period	Mean bias (K)	RMSD (K)	Matchups
D-J-F	DOISST	0.045 ± 0.003	0.428 ± 0.002	90247
	Model	-0.084 ± 0.004	0.563 ± 0.003	
M-A-M	DOISST	0.036 ± 0.001	0.383 ± 0.001	308448
	Model	-0.101 ± 0.001	0.389 ± 0.002	
J-J-A	DOISST	0.012 ± 0.003	0.483 ± 0.002	74107
	Model	-0.117 ± 0.003	0.486 ± 0.004	
S-O-N	DOISST	0.079 ± 0.003	0.429 ± 0.002	76157
	Model	-0.098 ± 0.004	0.590 ± 0.004	

411 **Table 5.** Summary statistics of DOISST and model outputs. Mean bias (K) and RMSD (K) are derived from temperature
412 differences against drifters' data during winter (D-J-F), spring (M-A-M), summer (J-J-A) and autumn (S-O-N) over the period
413 2019-2020. Each statistical parameter is associated with a 95% confidence interval computed through a bootstrap procedure
414 (Efron 1994).

415

416

417 The capability of DOISST to reproduce diurnal warming events is analysed in the following section.

418

419 **4.2.2 Diurnal warming events**

420 Diurnal warming (DW) can be defined as the difference between the SST at a given time of the day and the foundation SST
421 (see e.g. Minnett et al., 2019), i.e. the water temperature at a depth such that the daily variability induced by the solar irradiance
422 is negligible. In many cases, the foundation SST coincides with the night minimum SST, namely the temperature that is
423 recorded just before sunrise.

424 The capability of DOISST to describe diurnal warming events is analysed here in comparison with SEVIRI L3C, OSTIA
425 diurnal, model and drifter data. The evaluation is carried out by computing daily Diurnal Warming Amplitudes (DWAs) from
426 drifters and building a matchup dataset of DWAs as estimated from DOISST, SEVIRI L3C, OSTIA and model data. The
427 inclusion of SEVIRI data is mainly aimed at evaluating the impact of optimal interpolation on the input SEVIRI SSTs, while
428 OSTIA diurnal is used as intercomparison product The DWA is estimated here as a difference between the maximum occurred
429 during daytime (10:00-18:00 local time) and the minimum during nighttime (00:00-06:00 local time) (see also Takaya et al.,
430 2010; While et al., 2017). Explicitly, for each day (from 2019 to 2021) and for each drifter the two positions and times relative
431 to the minimum and maximum temperature are stored; over the same times and nearest positions, the temperatures of the other

432 datasets are stored too. The grid resolution of OSTIA diurnal (namely, 0.25° deg.) has been left unchanged since what is needed
433 is just the SST value at a given position, the nearest to the drifter's one.

434 The scatter plots of DOISST, SEVIRI, OSTIA, and model vs in situ-measured DWA have been computed for the years 2019-
435 2020 (Fig. 6) and organized during spring-summer and winter-autumn seasons (Fig. 7). This choice is aimed at comparing the
436 behaviour of the four products as a function of the seasons, since larger DWA intensities are expected in the spring-summer
437 period.

438 Overall, there is a good agreement between DOISST and drifter DWAs (Fig. 6a) as confirmed by an almost null mean bias (-
439 0.02 K), low RMSD (0.38 K) and high correlation coefficient (0.82). The largest DW amplitudes reach values as high as 4 K
440 in both DOISST and drifter data. SEVIRI (Fig. 6b) shows the same bias (-0.02 K) of DOISST in reconstructing DWAs but
441 higher RMSD (0.49 K) and lower correlation (0.74). It is relevant to note that the spread of SEVIRI DWAs around the line of
442 perfect agreement is reduced in DOISST, which coherently has a lower RMSD. The model (Fig. 6c) clearly underestimates
443 diurnal amplitudes larger than 1 K, and it is characterized by a high mean bias (-0.23 K) and RMSD (0.55 K), and lowest
444 correlation coefficient (0.66). Similarly, OSTIA diurnal (Fig. 6d) underestimates DWAs larger than 1 K, and it is characterized
445 by the highest mean bias (-0.28 K), RMSD of 0.54 K but shows less dispersion than the model around the line of perfect
446 agreement (correlation of 0.72).

447 The majority of DWA events lie between 0-1 K all over the year, but higher values are effectively reached during spring and
448 summer (Fig. 7). During these seasons, it appears more evident the capability of DOISST to better describe DWAs larger than
449 1 K (mean bias = -0.04 K; RMSD = 0.42 K; corr. = 0.83) compared to SEVIRI (mean bias = -0.05 K; RMSD = 0.53 K; corr.
450 = 0.76) and especially to the model (mean bias = -0.27 K; RMSD = 0.65 K; corr. = 0.63) and OSTIA diurnal (mean bias = -
451 0.39 K; RMSD = 0.66 K; corr. = 0.71). During winter and autumn, the overall statistics of the four products get better, clearly
452 due to the fact that the majority of DWA events range between 0-0.5 K. However, DWA events exceeding 1 K are also
453 observed, and such intense amplitudes are not found in the model-derived and OSTIA DWAs. Additionally, the good
454 agreement between DOISST and drifters still confirms that interpolated data do not suffer from the increased cloud cover
455 during winter and autumn periods.

456

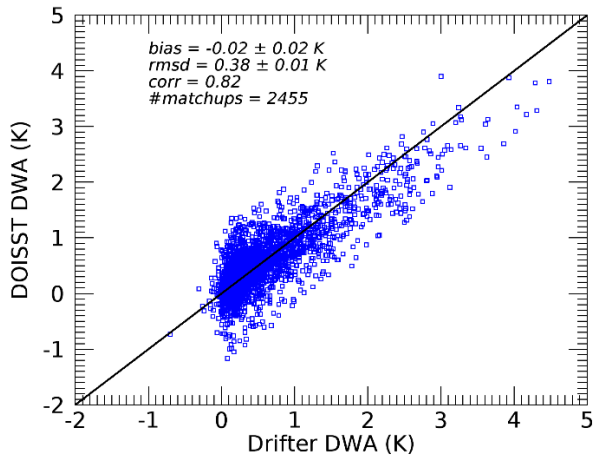
457

458

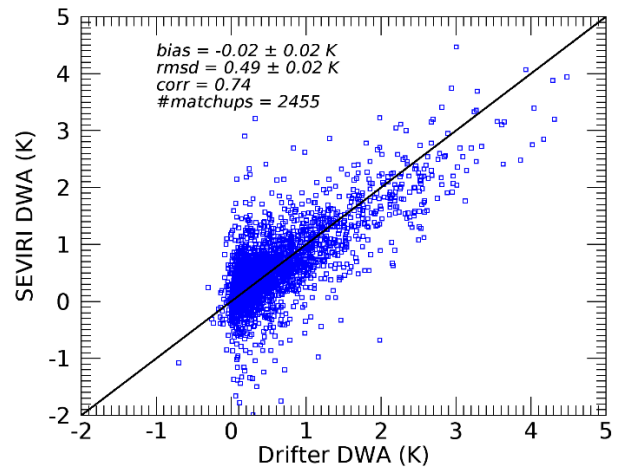
459

460

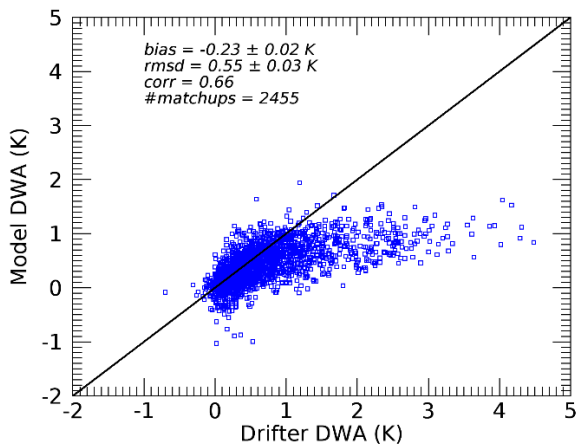
(a)



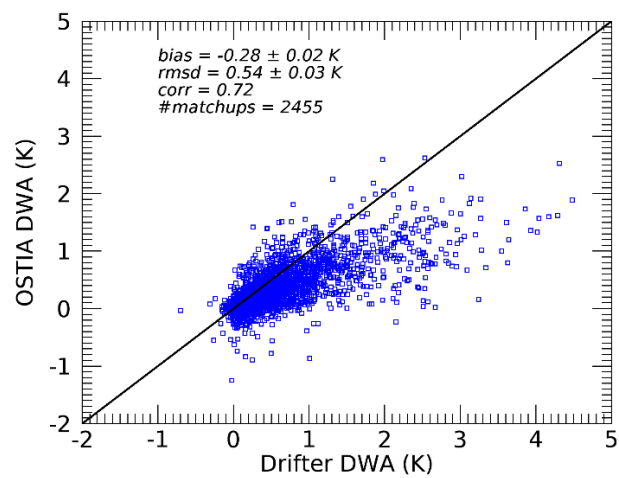
(b)



(c)



(d)



461 **Figure 6.** DWA scatter plots for (a) DOISST, (b) SEVIRI L3C, (c) model, and (d) OSTIA diurnal vs drifters over the period
462 2019-2020.

463

464

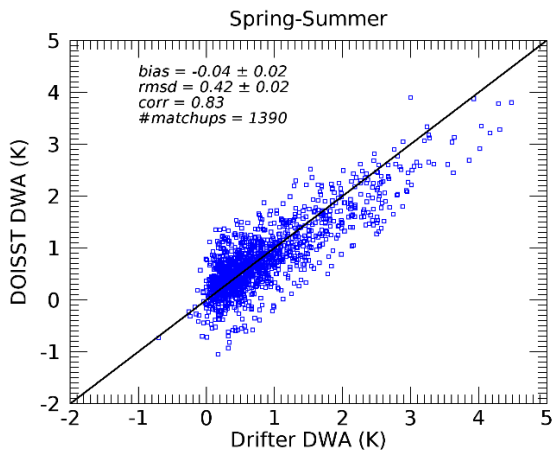
465

466

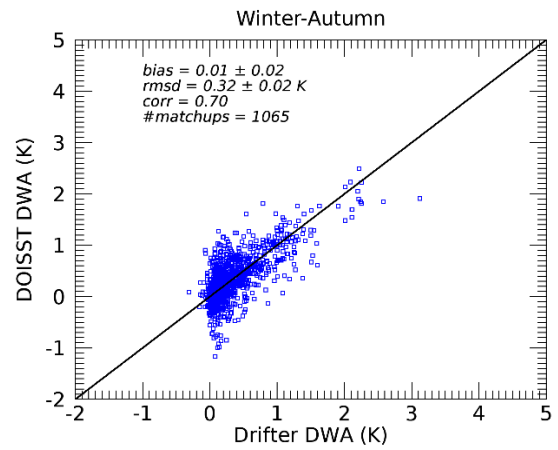
467

468

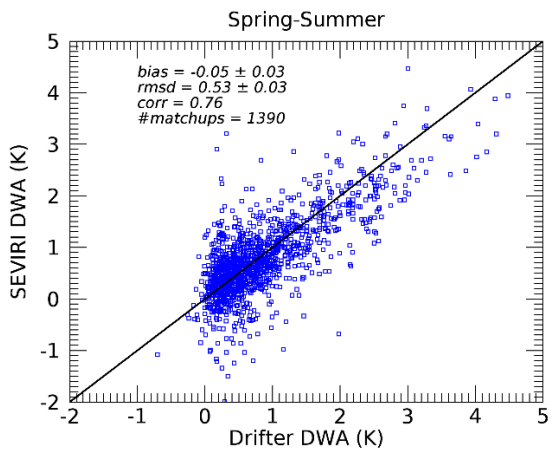
(a)



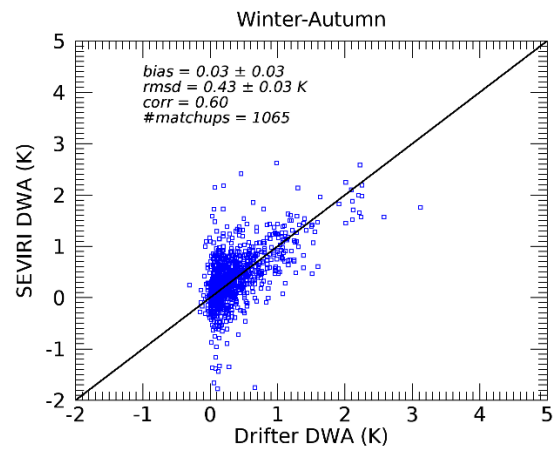
(b)



(c)

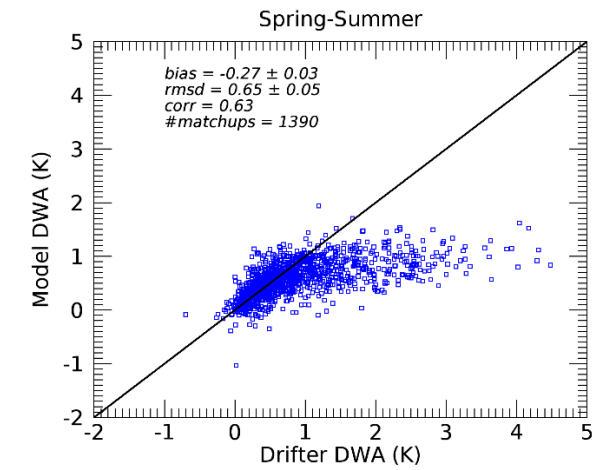


(d)

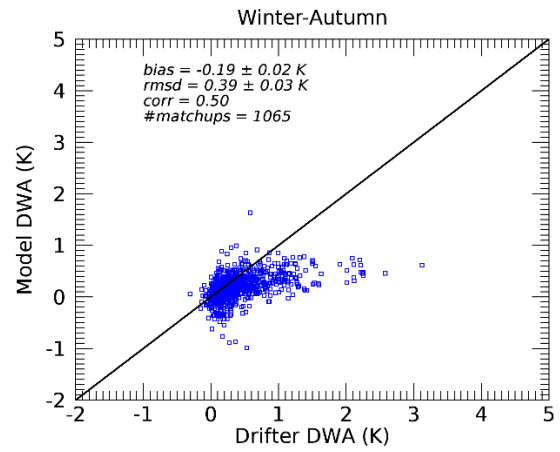


(e)

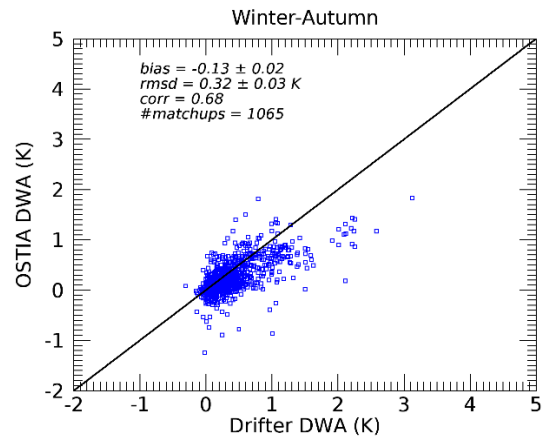
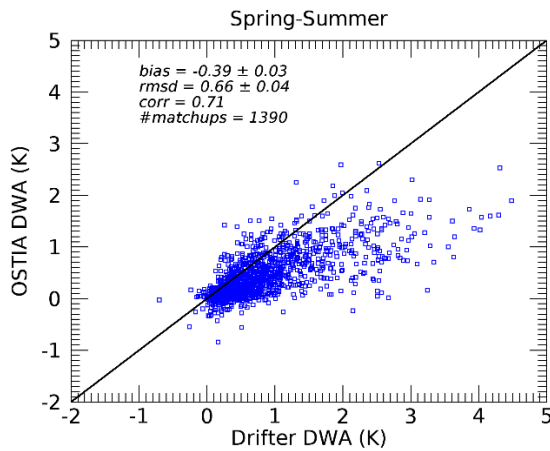
(f)



(g)



(h)



470

471 **Figure 7.** DWA scatter plots for DOISST (a,b), SEVIRI L3C (c,d), model (e,f), and OSTIA diurnal (g,h) vs drifters during
 472 Spring (M-A-M) and Summer (J-J-A), and Winter (D-J-F) - Autumn (S-O-N), over the period 2019-2020.

473

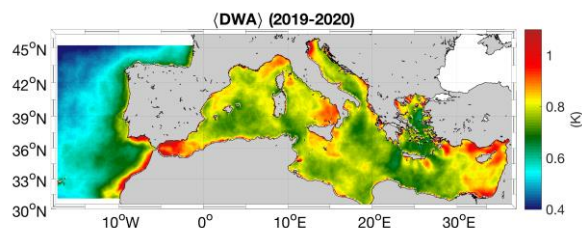
474 Having demonstrated the reliability of DOISST in the DWA estimate, we analyze its capability to reproduce the typical spatial
 475 variability and intensity of DW events in the Mediterranean Sea, a basin characterized by a frequent occurrence of intense DW
 476 events (Böhm et al., 1991; Buongiorno Nardelli et al., 2005; Gentemann et al., 2008; Merchant et al., 2008). In our investigation
 477 area, the 2019-2020 mean DWA ranges from a minimum of 0.4 K in the Atlantic ocean box off the Strait of Gibraltar, to a
 478 maximum of 1.2 K in several regions of the Mediterranean Sea (Fig. 8a) where individual diurnal warming events exceeding
 479 1 or even more than 2 K are quite frequent. The largest DWA were observed in the Levantine Basin, in the North Adriatic Sea
 480 and in correspondence with the Alboran Gyre. Less intense, though still remarkable, mean DWA patches reaching 0.9 K are
 481 found around the southern tip of the Italian Peninsula as well as in the coastal Ligurian Sea. In the same areas, it is found that

482 the frequency of DW events larger than 1 K and 2 K can reach up to 55% and 10% of the analyzed time series, respectively
483 (bearing in mind that our time series is given by the total number of days in 2019 and 2020) (Fig. 8b-c). The spatial variability
484 and magnitude of the DWA described by the DOISST product are consistent with past and recent studies on the SST diurnal
485 variability in the Mediterranean Area (Minnet et al. 2019; Marullo et al. 2016; Marullo et al. 2014).

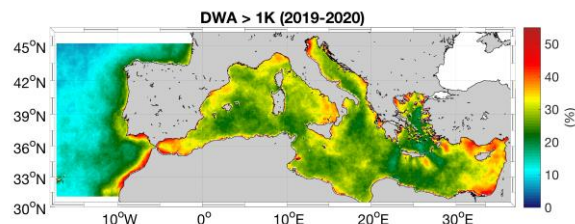
486

487 The magnitude of the maximum SST diurnal oscillation is also investigated. The spatial distribution of the maximum DWA
488 observed through 2019-2020 in the Mediterranean Sea (6°W to 36°E and 30°N to 46°N) (Fig. 8d) shows that the largest
489 amplitudes reach and exceed 3 K in 98% of the basin and local DWA patches exceeding 6 K are also ubiquitous, confirming
490 that the Mediterranean is one of the areas with the largest DWs of the global ocean (Minnet et al. 2019, and references therein).

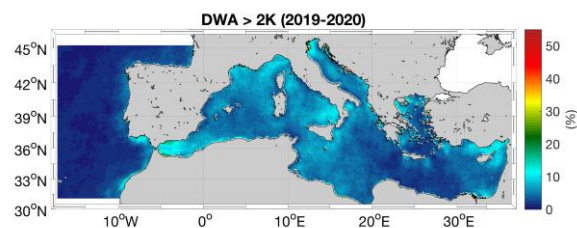
a)



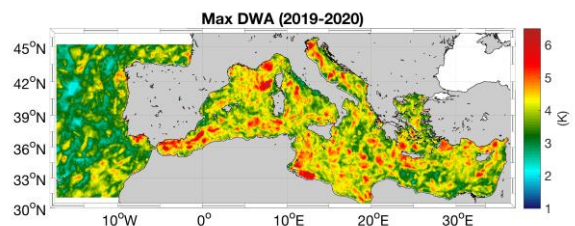
b)



c)



d)



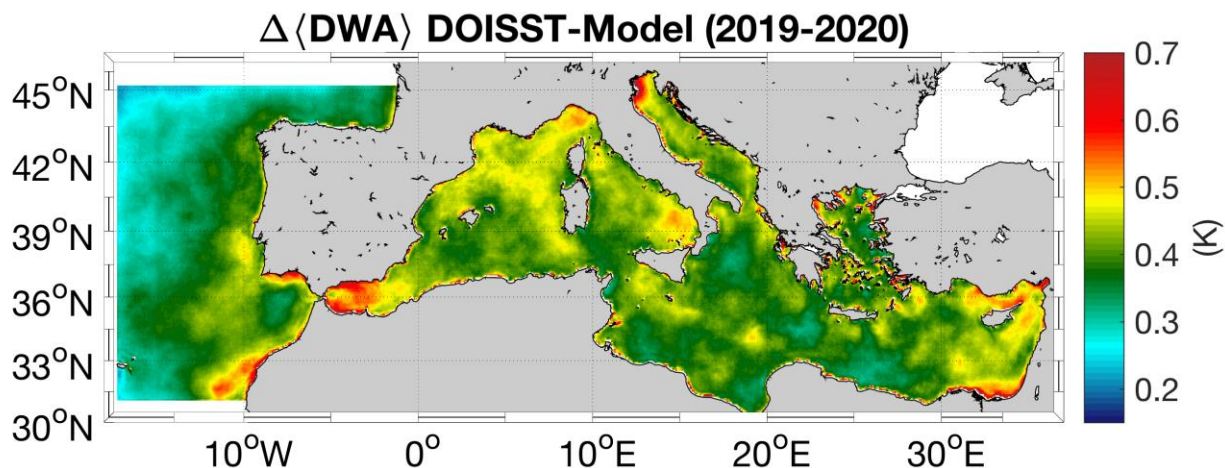
491

492 **Figure 8.** a) Mean diurnal warming amplitude (DWA) derived from DOISST; b) Percentage (over the total number of days in
493 the 2019-2020 period) of DOISST DWA larger than 1 K; c) Percentage of DOISST DWA larger than 2 K; d) Maximum
494 observed DOISST DWA. All the maps refer to the 2019-2020 period.

495

496 When compared to the model, DOISST exhibits mean DWAs with larger intensity than model outputs in all the locations of
497 the study area (Fig. 9). The ΔDWA , defined as DWA_{DOISST} minus DWA_{Model} , is always larger than 0.2 K and locally reaches
498 extreme values of ~ 1 K. The extent of the ΔDWA generally increases in areas where the DOISST mean DWA is larger, such

499 as in the Alboran Sea, Ligurian Sea, Levantine Basin and Southern Tyrrhenian, suggesting a tendency of the model to
500 underestimate the largest DW events.



501 **Figure 9.** Mean amplitude of the SST DW. Differences between the mean DWA seen by the DOISST product and the
502 model outputs (first layer).
503
504

505 **5 Data availability**

506 The Mediterranean diurnal optimal interpolated SST product is distributed as part of the CMEMS catalogue, and identified as
507 SST_MED_PHY_SUBSKIN_L4_NRT_010_036 (CMEMS product reference) and cmems_obs-sst_med_phy-
508 sst_nrt_diurnal-oi-0.0625deg_PT1H-m (CMEMS dataset reference) ([https://resources.marine.copernicus.eu/product-
509 detail/SST_MED_PHY_SUBSKIN_L4_NRT_010_036/INFORMATION](https://resources.marine.copernicus.eu/product-detail/SST_MED_PHY_SUBSKIN_L4_NRT_010_036/INFORMATION), last access: 03 November 2021,
510 https://doi.org/10.25423/CMCC/SST_MED_PHY_SUBSKIN_L4_NRT_010_036; Pisano et al, 2021). Access to the product
511 is granted after free registration as a user of CMEMS at <https://resources.marine.copernicus.eu/registration-form> (last access:
512 03 November 2021). Once registered, users can download the product through a number of different tools and services,
513 including the web portal Subsetter, Direct-GetFile (DGF) and FTP. A Product User Manual (PUM) and Quality Information
514 Document (QUID) are also available as part of the CMEMS documentation ([https://resources.marine.copernicus.eu/product-
515 detail/SST_MED_PHY_SUBSKIN_L4_NRT_010_036/DOCUMENTATION](https://resources.marine.copernicus.eu/product-detail/SST_MED_PHY_SUBSKIN_L4_NRT_010_036/DOCUMENTATION), last access: 03 November 2021). Eventual
516 updates of the product will be reflected in these documents. The basic characteristics of the DOISST product are summarized

517 in Table 2. The reduced subset used here for validation and review purposes is openly available at
518 <https://doi.org/10.5281/zenodo.5807729> (Pisano, 2021).

519

520 **6 Summary and conclusions**

521 A new operational Mediterranean diurnally varying SST product has been released (May 2021) within the Copernicus Marine
522 Environment Monitoring Service (CMEMS). This dataset provides optimally interpolated (L4) hourly mean maps of sub-skin
523 SST over the Mediterranean Sea at 1/16° horizontal resolution, covering the period from 1st January 2019 to near real time (1
524 day before real time) (Pisano et al., 2021). The diurnal optimal interpolated SST (DOISST) product is obtained from a blending
525 of hourly satellite (SEVIRI) data and model outputs via optimal interpolation, where the former are used as the observation
526 source and the latter as background. This method has been firstly proposed by Marullo et al. (2014), validated over one year
527 (2013) in Marullo et al. (2016), and implemented here operationally. The validation of the operational product was also
528 extended over two years (2019-2020).

529 In an ideal case, all data would be generated and compared at the same depth. Unfortunately, the first model layer is centered
530 at 1 m depth, while sub-skin SST is, by definition, representative of a depth of ~1 mm. In principle, it could be possible to
531 correct all the data, bringing them all to the same depth before any comparison or merging, by applying some model (see e.g.
532 Zeng et al., 1999). However, any correction algorithm would have added potential uncontrolled error sources (e.g., related to
533 ancillary data and/or to model assumptions) and implied significant additional operational efforts. For these reasons, rather
534 than trying to correct the first-guess bias, we preferred to leave it uncorrected, and focus on optimising the corrections driven
535 by available hourly satellite data.

536 DOISST proved to be rather accurate when compared to drifter measurements, and correctly reproduced the diurnal variability
537 in the Mediterranean Sea. The accuracy of DOISST results in an overall, almost null, mean bias of ~0.04 K and RMSD of
538 ~0.41 K (Table 3). This product is also more accurate than the input model, which shows a mean bias of ~-0.1 K and RMSD
539 of ~0.47 K. A warm (positive) and cold (negative) bias characterizes the DOISST and the model, respectively, also during
540 seasons (Fig. 5). These opposite biases are likely related to the different nature of the SST provided by DOISST, model and
541 drifter data, i.e. sub-skin (~1 mm from the surface), averaged 1 m depth and 20 cm depth, respectively, and then consistent
542 with the physical consequence of a reduction of the temperature with depth due to the vertical transfer heat process. The
543 DOISST RSMD generally keeps lower values compared to the model, ranging from a minimum of ~0.40 K (vs ~0.42 K for
544 the model) to a maximum of ~0.44 K (vs ~0.56 K for the model).

545 Compared to its native version (Marullo et al., 2016), the DOISST product maintains the same RMSD (estimated in 0.42 K)
546 but displays a lower mean bias (estimated as -0.10 K). The reduced bias could be ascribed to the fact that valid SEVIRI SST

547 values are always interpolated in DOISST, while they are left unchanged in the original method. Additionally, the DOISST
548 bias is comparable with that estimated for SEVIRI over the Mediterranean Sea (-0.03 K; Marullo et al. 2016), while the
549 DOISST RMSD is rather lower than SEVIRI one (0.47 K; Marullo et al. 2016). The DOISST bias is also lower than that of
550 the OSTIA diurnal product, which produces gap-free hourly mean fields of skin SST for the global ocean, and has been found
551 to underestimate the diurnal range of skin SST by 0.1-0.3 °C (While et al., 2017).

552 The analysis of the SST diurnal cycle as estimated from both DOISST, model and drifter data shows that the diurnal oscillation
553 in SST is well reconstructed by the DOISST while the model tends to underestimate this amplitude mainly during the central
554 warming hours (Fig. 4), and during spring and summer (Fig. 5). Specifically, DOISST overestimates the mean diurnal
555 amplitude by ~2.3% compared to that of drifters, while the model underestimates it by ~16%. This is particularly evident in
556 the analysis of diurnal warming (DW) events, where diurnal warming amplitudes (DWAs) as estimated by DOISST, model,
557 SEVIRI, and OSTIA diurnal data are compared vs drifter-derived DWAs. This analysis shows that amplitudes exceeding 1 K,
558 as measured by drifters, are well reconstructed by DOISST (Fig. 6a) with a mean bias of ~-0.02 K and RMSD of ~0.38 K. The
559 comparison with reconstructed SEVIRI DWAs (Fig. 6b) demonstrates that optimal interpolation does not change the SEVIRI
560 bias, which is practically null for both SEVIRI and DOISST (~-0.02 K), while it reduces the SEVIRI RMSD, from ~0.49 K
561 (SEVIRI) to ~0.38 K (DOISST). This is also evident in the reduction of the spread of SEVIRI DWAs around the line of perfect
562 agreement (Fig. 6b). Both the model and OSTIA diurnal underestimate DWAs when exceeding 1 K with a mean bias of ~-
563 0.23 K (model, Fig. 6c) and ~-0.28 K (OSTIA, Fig. 6d), and RMSD of ~0.55 K for both products.. This underestimation could
564 be related to several factors, such as that the vertical resolution of the model does not resolve the vertical temperature profile
565 within the warm layer. Yet, the physics and atmospheric forcing and/or the assimilation implemented in the model and OSTIA,
566 though different, are only partially able to resolve diurnal variations larger than 1 K. In any case, we can argue that the tendency
567 of the model to underestimate DWAs, mainly for amplitudes > 1 K, does not strongly impact the performance of DOISST in
568 reconstructing these amplitudes. This is likely due to two concurrent factors, the high accuracy of SEVIRI SST data and that
569 the Mediterranean area is particularly advantageous in terms of clear sky conditions.

570 Finally, the seasonal analysis also reveals that DOISST is not impacted by the different environmental conditions in the
571 Mediterranean Sea, in particular from the much frequent cloudiness during winter and autumn periods.

572 Overall, the DOISST product is able to accurately reconstruct the SST diurnal cycle, including diurnal warming events, for the
573 Mediterranean Sea and can thus represent a valuable dataset to improve the study of those processes that require sub-daily
574 frequency.

575
576
577
578

579 **Financial Support**

580 This work has been carried out within the Copernicus Marine Environment Monitoring Service (CMEMS) Sea Surface
581 Temperature Thematic Assembly Centre (SST TAC), contract n° 78-CMEMS-TAC-SST. This contract is funded by Mercator
582 Océan International as part of its delegation agreement with the European Union, represented by the European Commission,
583 to set-up and manage CMEMS.

584

585 **References**

586 Artale, V., Iudicone, D., Santoleri, R., Rupolo, V., Marullo, S., D'Ortenzo, F.; Role of surface fluxes in ocean general
587 circulation models using satellite sea surface temperature: validation of and sensitivity to the forcing frequency of the
588 Mediterranean thermohaline circulation; *J. Geophys. Res-Oceans*, 107(C8), 29-1–29-24,
589 <https://doi.org/10.1029/2000JC000452>, 2002

590 Bernie, D. J., Guilyardi, E., Madec, G., Slingo, J. M., Woolnough, S. J., and Cole, J. Impact of resolving the diurnal cycle in
591 an ocean–atmosphere GCM. Part 2: A diurnally coupled CGCM. *Clim. Dynam.*, 31(7), 909-925, DOI 10.1007/s00382-008-
592 0429-z, 2008

593 Böhm, E., Marullo, S., and Santoleri, R.. AVHRR visible-IR detection of diurnal warming events in the western Mediterranean
594 Sea, *Int. J. Remote Sens.*, , 12(4), 695-701, <https://doi.org/10.1080/01431169108929686>, 1991

595 Bowen, M. M., Emery, W. J., Wilkin, J. L., Tildesley, P. C., Barton, I. J., and Knewton, R.. Extracting multiyear surface
596 currents from sequential thermal imagery using the maximum cross-correlation technique, *J. Atmos. Ocean. Tech.*, 19(10),
597 1665-1676, [https://doi.org/10.1175/1520-0426\(2002\)019%3C1665:EMSCFS%3E2.0.CO;2](https://doi.org/10.1175/1520-0426(2002)019%3C1665:EMSCFS%3E2.0.CO;2), 2002.

598 Bretherton, F. P., Davis, R. E., and Fandry, C. B.. A technique for objective analysis and design of oceanographic experiments
599 applied to MODE-73. In *Deep Sea Research and Oceanographic Abstracts*, 23, 7, 559-582, [https://doi.org/10.1016/0011-
600 7471\(76\)90001-2](https://doi.org/10.1016/0011-7471(76)90001-2), 1976..

601 Buongiorno Nardelli, B.; Marullo, S.; Santoleri, R.. Diurnal Variations in AVHRR SST Fields: A Strategy for Removing
602 Warm Layer Effects from Daily Images. *Remote Sens. Environ.*, 95 (1), 47–56. <https://doi.org/10.1016/j.rse.2004.12.005>,
603 2005

604 Buongiorno Nardelli, B., Tronconi, C., Pisano, A., and Santoleri, R.. High and Ultra-High resolution processing of satellite
605 Sea Surface Temperature data over Southern European Seas in the framework of MyOcean project. *Remote Sens. Environ.*,
606 129, 1-16, <https://doi.org/10.1016/j.rse.2012.10.012>, 2013

607 Chen, S. S., and Houze Jr, R. A. Diurnal variation and life-cycle of deep convective systems over the tropical Pacific warm
608 pool. *Q. J. Roy. Meteor. Soc.*, 123(538), 357-388, <https://doi.org/10.1002/qj.49712353806>, 1997

609 Clayson, C. A., and Bogdanoff, A. S.. The effect of diurnal sea surface temperature warming on climatological air–sea fluxes.
610 *J. Climate*, 26(8), 2546-2556, <https://doi.org/10.1175/JCLI-D-12-00062.1>, 2013

611 Clementi, E., Oddo, P., Drudi, M., Pinardi, N., Korres, G., and Grandi A. Coupling hydrodynamic and wave models: first step
612 and sensitivity experiments in the Mediterranean Sea. *Ocean Dynam.*, 67(10), 1293-1312, [https://doi.org/10.1007/s10236-](https://doi.org/10.1007/s10236-017-1087-7)
613 [017-1087-7](https://doi.org/10.1007/s10236-017-1087-7), 2017

614 Clementi, E., Aydogdu, A., Goglio, A. C., Pistoia, J., Escudier, R., Drudi, M., Grandi, A., Mariani, A., Lyubartsev, V., Lecci,
615 R., Cretí, S., Coppini, G., Masina, S., & Pinardi, N.. Mediterranean Sea Physical Analysis and Forecast (CMEMS MED-
616 Currents, EAS6 system) (Version 1) [\[Data set\]](#). Copernicus Monitoring Environment Marine Service (CMEMS), 2021.Deser,
617 C., Alexander, M. A., Xie, S. P., and Phillips, A. S., Sea surface temperature variability: Patterns and mechanisms. *Annu. Rev.*
618 *Mar. Sci.* 2, 115-143, <https://doi.org/10.1146/annurev-marine-120408-151453>, 2010

619 Dobricic, S., and Pinardi, N.. An oceanographic three-dimensional variational data assimilation scheme. *Ocean Model.*, 22(3-
620 4), 89-105, <https://doi.org/10.1016/j.ocemod.2008.01.004>, 2008

621 Efron, B.; Tibshirani, R.J. *An Introduction to the Bootstrap*; CRC Press: Boca Raton, FL, USA, 1994.

622 Fiedler, E. K., McLaren, A., Banzon, V., Brasnett, B., Ishizaki, S., Kennedy, J., ... and Donlon, C. Intercomparison of long-
623 term sea surface temperature analyses using the GHRSSST Multi-Product Ensemble (GMPE) system. *Remote Sens. Environ.*,
624 222, 18-33, <https://doi.org/10.1016/j.rse.2018.12.015>, 2019

625 Gentemann, C. L. Minnett, P. J., Le Borgne, P., and Merchant, C. J. Multi-satellite measurements of large diurnal warming
626 events. *Geophysical Research Letters*, 35 (22), L22602. <http://dx.doi.org/10.1029/2008GL035730>,
627 <https://doi.org/10.1029/2008GL035730>, 2008

628 Good, S. A., Corlett, G. K., Remedios, J. J., Noyes, E. J., and Llewellyn-Jones, D. T.. The global trend in sea surface
629 temperature from 20 years of advanced very high resolution radiometer data. *J. Climate*, 20(7), 1255-1264,
630 <https://doi.org/10.1175/JCLI4049.1>, 2007 Good, S., Fiedler, E., Mao, C., Martin, M.J., Maycock, A., Reid, R., Roberts-Jones,
631 J., Searle, T., Waters, J., While, J., and Worsfold, M.. The Current Configuration of the OSTIA System for Operational
632 Production of Foundation Sea Surface Temperature and Ice Concentration Analyses. *Remote Sens.-BASEL*, 12(4),720,
633 <https://doi.org/10.3390/rs12040720>, 2020.

634 Huang, B., Liu, C., Freeman, E., Graham, G., Smith, T., & Zhang, H. M.. Assessment and Intercomparison of NOAA Daily
635 Optimum Interpolation Sea Surface Temperature (DOISST) Version 2.1. *J. Climate*, 34(18), 7421-7441.

636 Kotsias, G., & Lolis, C. J.. A study on the total cloud cover variability over the Mediterranean region during the period 1979–
637 2014 with the use of the ERA-Interim database. *Theor. Appl. Climatol.*, 134(1), 325-336, [https://doi.org/10.1175/JCLI-D-21-](https://doi.org/10.1175/JCLI-D-21-0001.1)
638 [0001.1](https://doi.org/10.1175/JCLI-D-21-0001.1), 2018

639 Le Traon, P. Y., Reppucci, A., Alvarez Fanjul, E., Aouf, L., Behrens, A., Belmonte, M., ... and Zacharioudaki, A. From
640 observation to information and users: The Copernicus Marine Service perspective. *Frontiers in Marine Science*, 6, 234,
641 <https://doi.org/10.3389/fmars.2019.00234>, 2019.

642 Marullo, S., Minnett, P. J., Santoleri, R., and Tonani, M.. The diurnal cycle of sea-surface temperature and estimation of the
643 heat budget of the Mediterranean Sea. *J. Geophys. Res.-Oceans*, 121(11), 8351-8367, <https://doi.org/10.1002/2016JC012192>,
644 2016Marullo, S., Santoleri, R., Ciani, D., Le Borgne, P., Péré, S., Pinardi, N., Tonani, M., and Nardone, G.. Combining model
645 and geostationary satellite data to reconstruct hourly SST field over the Mediterranean Sea. *Remote Sens. Environ.*, 146, 11-
646 23, <https://doi.org/10.1016/j.rse.2013.11.001>, 2014

647 Merchant, C. J., Embury, O., Bulgin, C. E., Block, T., Corlett, G. K., Fiedler, E., ... and Donlon, C.. Satellite-based time-series
648 of sea-surface temperature since 1981 for climate applications. *Scientific data*, 6(1), 1-18, 2019.

649 Merchant, C. J., Filipiak, M. J., Le Borgne, P., Roquet, H., Autret, E., Piollé, J. F., & Lavender, S. . Diurnal warm-layer events
650 in the western Mediterranean and European shelf seas. *Geophys. Res. Lett.*, 35(4), <https://doi.org/10.1029/2007GL033071>,
651 2008

652 Minnett, P. J., Alvera-Azcárate, A., Chin, T. M., Corlett, G. K., Gentemann, C. L., Karagali, I., ... and Vazquez-Cuervo, J. .
653 Half a century of satellite remote sensing of sea-surface temperature. *Remote Sens. Environ.*, 233, 111366,
654 <https://doi.org/10.1016/j.rse.2019.111366>, 2019

655 Oddo, P., Adani, M., Pinardi, N., Fratianni, C., Tonani, M., and Pettenuzzo, D. A Nested Atlantic-Mediterranean Sea General
656 Circulation Model for Operational Forecasting. *Ocean Sci. Discuss.*, 5(4), 461-473, <https://doi.org/10.5194/os-5-461-2009>,
657 2009.

658 Oddo, P., Bonaduce, A., Pinardi, N., and Guarneri, A. Sensitivity of the Mediterranean sea level to atmospheric pressure and
659 free surface elevation numerical formulation in NEMO. *Geosci. Model Dev.*, 7, 3001–3015, [https://doi.org/10.5194/gmd-7-](https://doi.org/10.5194/gmd-7-3001-2014)
660 [3001-2014](https://doi.org/10.5194/gmd-7-3001-2014), 2014.

661 Oliver, E. C., Benthuisen, J. A., Darmaraki, S., Donat, M. G., Hobday, A. J., Holbrook, N. J., ... and Sen Gupta, A. . Marine
662 heatwaves. *Annu. Rev. Mar. Sci.*, 13, 313-342, <https://doi.org/10.1146/annurev-marine-032720-095144>, 2021Pinardi, N.,

663 Allen, I., De Mey, P., Korres, G., Lascaratos, A., Le Traon, P.Y., Maillard, C., Manzella G., and Tziavos, C. . The
664 Mediterranean ocean Forecasting System: first phase of implementation (1998-2001). *Ann. Geophys.*, 21, 1, 3-20,
665 <https://doi.org/10.5194/angeo-21-3-2003>, 2003.

666 Pisano, A., Marullo, S., Artale, V., Falcini, F., Yang, C., Leonelli, F. E., ... and Buongiorno Nardelli, B.. New evidence of
667 mediterranean climate change and variability from sea surface temperature observations. *Remote Sens.-BASEL*, 12(1), 132,
668 <https://doi.org/10.3390/rs12010132>, 2020

669 Pisano, A., Buongiorno Nardelli, B., Marullo, S., Rosalia, S., Tronconi, C., & Ciani, D. (2021). Mediterranean Sea - High
670 Resolution Diurnal Subskin Sea Surface Temperature Analysis (Version 1) [Data set]. Copernicus Marine Environment
671 Monitoring Service (CMEMS). https://doi.org/10.25423/CMCC/SST_MED_PHY_SUBSKIN_L4_NRT_010_036

672 Pisano, Andrea. (2021). CNR Mediterranean Sea High Resolution Diurnal Subskin Sea Surface Temperature Analysis:
673 Validation subset. <https://doi.org/10.5281/zenodo.5807729>

674 Reverdin, G., Boutin, J., Martin, N., Lourenço, A., Bouruet-Aubertot, P., Lavin, A., ... and Lazure, P.. Temperature
675 measurements from surface drifters. *J. Atmos. Ocean.Tech.* 27(8), 1403-1409, <https://doi.org/10.1175/2010JTECHO741.1>,
676 2010.

677 Rio, M. H., and Santoleri, R.. Improved global surface currents from the merging of altimetry and sea surface temperature
678 data. *Remote Sens. Environ.*, 216, 770-785, <https://doi.org/10.1016/j.rse.2018.06.003>, 2018

679 Storto, A., and Oddo, P. . Optimal assimilation of daytime SST retrievals from SEVIRI in a regional ocean prediction system.
680 *Remote Sens.-BASEL*, 11(23), 2776, <https://doi.org/10.3390/rs11232776>, 2019

681 Takaya, Y., Bidlot, J. R., Beljaars, A. C., & Janssen, P. A.. Refinements to a prognostic scheme of skin sea surface temperature.
682 *J Geophys. Res-Oceans*, 115(C6), <https://doi.org/10.1029/2009JC005985>, 2010

683 Yang, C., Leonelli, F. E., Marullo, S., Artale, V., Beggs, H., Nardelli, B. B., ... and Pisano, A.. Sea Surface Temperature
684 Intercomparison in the Framework of the Copernicus Climate Change Service (C3S). *J. Climate*, 34(13), 5257-5283,
685 <https://doi.org/10.1175/JCLI-D-20-0793.1>, 2021

686 Waters, J., Lea, D. J., Martin, M. J., Mirouze, I., Weaver, A., and While, J.. Implementing a variational data assimilation
687 system in an operational 1/4 degree global ocean model. *Q. J. Roy. Meteor. Soc.*, 141(687), 333-349,
688 <https://doi.org/10.1002/qj.2388>, 2015

689 While, J., Mao, C., Martin, M. J., Roberts-Jones, J., Sykes, P. A., Good, S. A., and McLaren, A. J.. An operational analysis
690 system for the global diurnal cycle of sea surface temperature: implementation and validation. *Q. J. Roy. Meteor. Soc.*,

691 143(705), 1787-1803, <https://doi.org/10.1002/qj.3036>, 2017.Zeng, X., Zhao, M., Dickinson, R. E., & He, Y.. A multi-year
692 hourly sea surface skin temperature dataset derived from the TOGA TAO bulk temperature and wind speed over the tropical
693 Pacific. *J. Geophys. Res-Oceans*, 104, 1525–1536, <https://doi.org/10.1029/1998JC900060>, 1999

694 Zeng, X., Zhao, M., Dickinson, R. E., & He, Y. (1999). A multi-year hourly sea surface skin temperature dataset derived from
695 the TOGA TAO bulk temperature and wind speed over the tropical Pacific. *J. of Geophysical Res.*, 104, 1525–1536.

696

697

698



699

700